IOP Publishing Journal of Physics B: Atomic, Molecular and Optical Physics

J. Phys. B: At. Mol. Opt. Phys. **47** (2014) 042001 (30pp) doi:10.1088/0953-4075/47/4/042001

Topical Review

Coherent electron emission from simple molecules by impact of energetic charged particles*

M F Ciappina[1,2], O A Fojón[3] and R D Rivarola[3]

[1] ICFO - Institut de Ciències Fotòniques, E-08860 Castelldefels (Barcelona), Spain
[2] Department of Physics, Auburn University, Auburn, Alabama 36849, USA
[3] Laboratorio de Colisiones Atómicas and Instituto de Física Rosario, CONICET-UNR, Avenida Pellegrini 250, 2000 Rosario, Argentina

E-mail: mfc0007@auburn.edu

Received 18 July 2013, revised 5 December 2013
Accepted for publication 5 December 2013
Published 4 February 2014

Abstract

We review the theoretical and experimental progress in the field of coherent electron emission from simple molecules by the impact of energetic charged particles. We describe in detail the different theoretical approaches to tackle the single ionization of diatomic molecules by the impact of ions and electrons. Furthermore, we compare with experimental measurements, where available. The case of photon impact is also considered, in order to obtain a deeper understanding of the physics involved. An attempt is made to emphasize the phenomenology behind these molecular processes and to discuss the advantages and drawbacks of the different theoretical approaches. Additionally, we highlight the differences and similarities between the particular projectiles which initiate the process, namely ions, electrons or photons.

Keywords: collisions, molecular targets, ionization, coherence, interference effects

(Some figures may appear in colour only in the online journal)

1. Introduction

A controversy remained for centuries in the physical community inquiring whether light is composed of corpuscles or if it possesses intrinsically a wave nature. Newton thought that the rays of light were built up by tiny corpuscles emitted from shining bodies even if this was in conflict with some known phenomena at his time and that we attribute nowadays to interferences. Interestingly, in the same period Christiaan Huygens and other scientists judged that light consists of traveling waves but the overpowering Newton's authority ruled until the double-slit experiment performed by Thomas Young in the initial years of 1800 demonstrated unambiguously the wave character of light [1]. He showed that light passing through two closely separated lines traced on an opaque glass creates, when projected over a wall, an interference pattern: an alternation of bright and dark strips. However, Max Planck in *an act of desperation* postulated the quantized nature of the electromagnetic radiation in 1901 to explain the black-body spectra, and soon after Albert Einstein with his description of the photoelectric effect in 1905, returned to support the corpuscular posture. Contributing even more to the controversy, Arthur Compton performed in 1923 a series of scattering experiments with high-energy radiation backing the idea that light is made up of particles that, after Gilbert Lewis [2], we call nowadays photons. A reconciliation between all these contradictory findings came after the wave–particle duality principle, first introduced by Louis de Broglie in 1924, and valid not only for photons but for every quantum object. This duality configures the core of quantum mechanics, being one of the most remarkable conceptual deviations from classical physics. Soon after, the famous experiment of Clinton

* This review is in memorial of Professor Uwe Becker (1947–2013), who inspired us during the writing of this work.

Davidson and Lester Garmer in 1927 confirmed the de Broglie hypothesis.

Many electron diffraction or double-slit type experiments were performed since the 1960s with electrons [3–8] and even larger quantum objects such as C_{60} fullerenes (buckyballs) [9]. In Feynman's words, electron diffraction *contains the only mystery. In telling you how it works we will have told you about the basic peculiarities of all quantum mechanics*. The Heisenberg uncertainty principle, indeed, lies behind all these experiments. As is well-known, it imposes constrains to the precision of simultaneous measurements of the position and momentum of quantum objects in contrast with classical physics where this simultaneity is entirely possible. In order to obtain an interference pattern, the momentum of the quantum object must be so precisely determined that its position is delocalized by more than the slit width. If this delocalization is dropped out, decoherence occurs and the interference pattern disappears [10]. Whether it is possible to determine through which slit an object passes without losing interference patterns is a never ending proposition that continues to be the matter of research and maybe controversy in the present days too. In particular, a thought experiment proposed by Feynman in 1965 has been brought to life just during the completion of this work [11].

Another fascinating mechanism related to double-slit experiments is the coherent superposition of quantum objects emitted from spatially separated positions. This is often referred to as *the molecular double-slit scenario* [10] in which a homonuclear diatomic molecule such as molecular hydrogen [12] or nitrogen [13] is ionized by irradiation with light or by impact of charged particles such as electrons or heavy ions. These processes have received special attention for decades due to their intrinsic importance in areas such as astrophysics and biology (see e.g. [14] for more details). The existence of interference effects for these reactions was first recognized by Howard Cohen and Ugo Fano in 1966 in theoretical studies of photoionization of N_2 and O_2 molecules [15]. They showed that an oscillating pattern appeared in the partial photoionization cross sections (PCS) when a two-centre electron wavefunction was employed to describe the coherent electron emission from both atomic sites. Electrons can be emitted coherently from both of the atoms in these molecules in such a way that the electron waves could be either in phase or out of phase. Consequently, these systems should exhibit an interference behaviour equivalent to that seen in macroscopic double-slit experiments. Nevertheless, the first experimental clear proof for these interference phenomena was given more than three decades later, in 2001, in the single ionization of H_2 molecules by impact of Kr^{34+} projectiles. Starting from this seminal work by Stolterfoht *et al* [12], about coherent electron emission from H_2 molecules by impact of highly charged ions impact, there has been an incessant activity in the field (since then, the article has received around 150 citations and counting).

With the constant advance of experimental capabilities in atomic physics, measurements on few-body fragmentation processes, such as single and double ionization by charged particle impact or mutual ionization of both collision partners, have become much more complex. Especially cold target recoil ion momentum spectroscopy (COLTRIMS) techniques, also known as reaction microscopes, have led to a new generation of atomic collision experiments (for a review see e.g. [16]). Kinematically complete experiments are now feasible for a broad range of projectiles and kinematical conditions and studies about the coherent emission of electrons from atomic centres are of great interest and could trigger new experiments and theoretical investigations [17].

One additional point that deserves to be explored, in principle theoretically, is the possibility to perform single ionization experiments with aligned molecules. We consider the pump-probe techniques—used extensively in laser driven experiments—have reached high maturity and they could be adapted to align molecules, before projectile beams initiate the electron dynamics.

We start this review with the theoretical description of single ionization of simple molecules by heavy-ion impact (section 2). Special emphasis is put on the distorted wave models and comparisons with the most relevant experiments are carried out. In section 3, we continue our timeline with the theoretical description of single ionization of simple molecules initiated by electrons. Here, particular stress is set on first-order theories able to deal with electron impact and also comparisons with experiments are presented. Finally, we give in section 4 a brief summary of theories and experiments of photon-induced single ionization of simple molecules. The review ends with our conclusions and an outline of possible future experiments with aligned molecules. Atomic units are used throughout unless otherwise stated.

2. Ion beam projectiles

We begin by considering the case of fast bare ion beams of nuclear charge Z_p impinging on simple molecular targets. Fast in our context implies the projectile velocity is much larger, but still within the non-relativistic domain, than the typical bound electron velocity. In particular, the interest of this work is focused on the process of *single* ionization. At high enough collision energies, for which the collision time is smaller than the relaxation one, corresponding to the passive electrons—those electrons that remain bound to the molecule acting as spectators—we can assume in a good approximation that they stay frozen in their respective molecular orbitals during the reaction. Moreover, we could also suppose that the collision time is also shorter than the vibrational and rotational ones, and consequently the orientation of the molecule remains fixed in the space until the direct interaction of the projectile with the target ends. For instance, for the projectile velocities we use and considering small molecules, the collision time τ is of the order of sub-fs to -as (1 fs $= 10^{-15}$ s, 1 as $= 10^{-18}$ s), while the typical vibration and rotational frequencies are in the range of $10^{13} \sim 10^{14}$ Hz and $10^{10} \sim 10^{12}$ Hz, respectively (see e.g. [18]). The adequacy of these assumptions has been tested for numerous aggregates, including atoms and molecules (see e.g. [19] and [20]).

Following the main ideas introduced for single electron capture from atomic targets by Rivarola *et al* [21], Fainstein *et al* [22] demonstrated for single ionization that using the

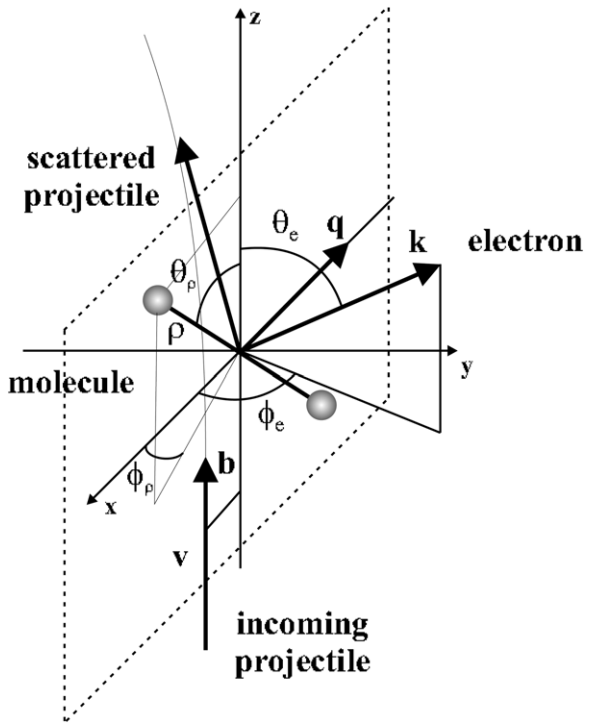

Figure 1. Coordinate system, angles and quantities used for the case of heavy ions. The z-axis is parallel to the direction of the incoming projectile and the x–z plane defines the so-called scattering plane. The internuclear axis $\boldsymbol{\rho}$ of the diatomic molecule subtends a polar angle θ_ρ (angle with respect to the z-axis) and an azimuthal angle ϕ_ρ (angle with respect to the x-axis).

straight line version of the impact parameter approximation—where the projectile is assumed to describe a classical trajectory while the light particles, the electrons, present a quantum-mechanical behaviour—the multielectronic nature of problem can be reduced and a monoelectronic treatment can be invoked, i.e. where only one *active* electron takes part of the process. This result was then extended for electron capture in molecular targets by Corchs *et al* [23] and for electron ionization reactions by Galassi *et al* [24], respectively.

Let us first focus our interest on the single ionization of diatomic molecules by an impact of projectiles with charge Z_p and incoming velocity $\mathbf{v}$. The geometry of the collision system is shown in figure 1. An incoming projectile beam is directed along the z-axis and we define the $x-z$ plane as the scattering plane. The momentum transfer $\mathbf{q}$ is given by $\mathbf{q} = \mathbf{K}_i - \mathbf{K}_f$ where $\mathbf{K}_i$ ($\mathbf{K}_f$) is the initial (final) momentum of the incident (scattered) particle. The momentum $\mathbf{k}$ of the ionized electron is represented in usual spherical coordinates by the angles θ_e and ϕ_e. Finally, θ_ρ defines the orientation of the internuclear axis $\boldsymbol{\rho}$ with respect to the z-axis (the polar angle) and ϕ_ρ is the azimuthal angle, i.e. the angle with respect to the x-axis. The transition amplitude per ionized electron, as a function of the impact parameter $\mathbf{b}$, with respect to the centre of mass of the target, can thus be expressed as (for details see Fainstein *et al* [22] and Galassi *et al* [24]):

$$\mathcal{A}_{fi}(\mathbf{b},\boldsymbol{\rho}) = \left(\prod_{j=1}^{2} b_j^{2iZ_pZ_j/v}\right) \exp\left(-\frac{2i}{v}\int_0^\infty V_s(\mathbf{R},\boldsymbol{\rho})\,dR\right) \times a_{fi}(\mathbf{b},\boldsymbol{\rho}), \tag{1}$$

where $\mathbf{b}_j$ is the impact parameter with respect to the j-nucleus of the molecule of charge Z_j, the upper limit in the $\prod$ symbol is the number of molecular centres, $\mathbf{R}$ is the vector that gives the relative position of the projectile with respect to the centre of mass of the nuclei of the molecule and $V_s(\mathbf{b},\boldsymbol{\rho})$ is a static potential which takes into account the interaction between the projectile and the passive electrons averaged on their orbital distributions. The term $\left(\prod_{j=1}^{2} b_j^{2iZ_pZ_j/v}\right)$ in equation (1) contains all the information associated with the interactions of the projectile with the nuclei of the molecule and $a_{fi}(\mathbf{b},\boldsymbol{\rho})$ is a purely electronic transition amplitude.

The corresponding T-matrix element, function on the transverse momentum $\boldsymbol{\eta}$ transferred by the projectile to the target and on the molecular orientation, is related to the transition amplitude $\mathcal{A}_{fi}(\mathbf{b},\boldsymbol{\rho})$ through the two-dimensional Fourier transform:

$$T_{fi}(\boldsymbol{\eta},\boldsymbol{\rho}) = iv\int d\mathbf{b}\exp(i\boldsymbol{\eta}\cdot\mathbf{b})\,\mathcal{A}_{fi}(\mathbf{b},\boldsymbol{\rho}). \tag{2}$$

In the centre of mass of the complete system, the fully differential cross section per orbital is given by the expression:

$$\frac{d^4\sigma}{dE_k\,d\Omega_k\,d\Omega_\rho\,d\Omega_s} = N_e(2\pi)^4\mu_i^2 k\frac{K_f}{K_i}|T_{fi}(\boldsymbol{\eta},\boldsymbol{\rho})|^2\delta(E_f-E_i). \tag{3}$$

In equation (3) the momentum and energy of the ejected electron are given by $\mathbf{k}$ and E_k, respectively, μ_i is the reduced mass of the projectile-target system in the initial channel, N_e is the number of electrons in the considered molecular orbital (MO) and E_i (E_f) is the initial (final) energy of the complete system. In addition, $d\Omega_\rho = \sin\theta_\rho\,d\theta_\rho\,d\phi_\rho$ indicates the solid angle associated with the molecular axis orientation and $d\Omega_s = \sin\theta_s\,d\theta_s\,d\phi_s$ and $d\Omega_k = \sin\theta_e\,d\theta_e\,d\phi_e$ denote the solid angles subtended by the scattered particle and the ionized electron in the final channel, respectively.

We can also define the fully differential cross section under the form:

$$\frac{d^4\sigma}{d\mathbf{k}\,d\boldsymbol{\eta}\,d\Omega_\rho} = N_e(2\pi)^4|T_{fi}(\boldsymbol{\eta},\boldsymbol{\rho})|^2\delta(E_f-E_i). \tag{4}$$

The triply differential cross section $d^3\sigma/dE_k\,d\Omega_k\,d\Omega_\rho$ may be obtained by integrating the expression (3) on the solid angle $d\Omega_s$. After some algebra it can be shown that (see for example Stolterfoht *et al* [20]):

$$\frac{d^3\sigma}{dE_k\,d\Omega_k\,d\Omega_\rho} = N_e k\int d\mathbf{b}|\mathcal{A}_{fi}(\mathbf{b},\boldsymbol{\rho})|^2 = N_e k\int d\mathbf{b}|a_{fi}(\mathbf{b},\boldsymbol{\rho})|^2. \tag{5}$$

As can be immediately concluded from equations (1) and (5), the interactions of the projectile with the target nuclei and with the passive electrons, which are present under the integral symbol as exponential phases, do not affect the calculation of $d^3\sigma/dE_k\,d\Omega_k\,d\Omega_\rho$.

Moreover, using the Parseval identity, it can be found that

$$\frac{d^3\sigma}{dE_k\,d\Omega_k\,d\Omega_\rho} = N_e k\int d\mathbf{b}|a_{fi}(\mathbf{b},\boldsymbol{\rho})|^2 = N_e(2\pi)^4\frac{k}{v^2}\int d\boldsymbol{\eta}|\tilde{T}_{fi}(\boldsymbol{\eta},\boldsymbol{\rho})|^2, \tag{6}$$

where $\tilde{T}_{fi}(\boldsymbol{\eta}, \boldsymbol{\rho})$ is obtained from equation (2) using $a_{fi}(\mathbf{b}, \boldsymbol{\rho})$ instead of $\mathcal{A}_{fi}(\mathbf{b}, \boldsymbol{\rho})$ in the integrand. We should note that within the perturbative framework the expressions above obtained are of general validity, being independent of the particular perturbative theoretical model used to calculate the scattering T-matrix element. Just to cite a couple of examples, in [25, 26] a continuum distorted wave - eikonal initial state (CDW-EIS) approximation with the MO of the continuum calculated using a Schwinger variational iterative method is employed to study the single ionization of the hydrogen molecule by different bare heavy ions and in [28] triply differential cross sections (TDCS) and doubly differential cross sections (DDCS) for the single ionization of H_2 by proton impact, using the molecular three-body distorted-wave–eikonal initial-state (M3DW-EIS) approach, are presented. In addition, TDCS were calculated with a semiclassical version of the first-order Born approximation by Járai-Szabó *et al* [27]. On the other hand, non-perturbative models, mainly based on the solution of the time-dependent Schrödinger equation (TDSE) for the active electron combined with a semiclassical scheme for the incoming projectile, were also developed (see e.g. [29, 30]).

In the following, and in order to describe the dynamics of the active electron, we will revisit mainly the results obtained within the CDW-EIS approximation, introduced by Crothers and McCann [31] for monoelectronic targets and then extended to the multielectronic ones (see e.g. Fainstein *et al* [22]; Gulyás *et al* [32]; Galassi *et al* [24]).

The active electron-scattering matrix element can be written under the forms:

$$\tilde{T}_{fi}^{+} = \langle \chi_f^{-} | (H - E)^{\dagger} | \Psi_i^{+} \rangle \tag{7}$$

and

$$\tilde{T}_{fi}^{-} = \langle \Psi_f^{-} | (H - E) | \chi_i^{+} \rangle, \tag{8}$$

corresponding to the post and prior versions, respectively. In these two last expressions and using the fact that $M_P \gg 1$ and $M_T \gg 1$ (with M_P and M_T as the masses of the projectile and target nuclei, respectively), the Hamiltonian H can be written as

$$H = -\frac{\nabla_{R_i}^2}{2\mu_i} - \frac{\nabla_x^2}{2} - \sum_{j=1}^{n} \frac{Z_j}{x_j} - \frac{Z_P}{s} + V_{ap}(x) \tag{9}$$

where $V_{ap}(x)$ is a Hartree–Fock type potential that describes the interaction of the active and passive electrons, averaged on the coordinate space distribution of the latter ones. With $\mathbf{x}$ and $\mathbf{s}$ we indicate the position of the active electron with respect to the target centre of mass and to the projectile, respectively, and with $\mathbf{x}_j$ the position of this electron relative to each one of the nuclei of the molecule. Finally, $\mathbf{R}_i$ denotes the position of the projectile with respect to the centre of mass of the target. In equations (7) and (8), Ψ_i^{+} and Ψ_f^{-} are exact solutions of the Schrödinger equations:

$$(H - E)\Psi_i^{+} = 0 \tag{10}$$

$$(H - E)\Psi_f^{-} = 0 \tag{11}$$

with correct outgoing, equation (10), and incoming, equation (11), asymptotic boundary conditions, respectively. Furthermore, we define χ_i^{+} and χ_f^{-} as initial and final active-electron distorted wavefunctions which preserve correct boundary conditions in the entry and exit channel, respectively. This is a fundamental aspect to take into account in the formulation of perturbative series when Coulomb interaction potentials are considered, to avoid the presence of divergences in the transition amplitudes coming from the population of intermediate elastic channels [33].

In the CDW-EIS approximation, χ_i^{+} is chosen as

$$\chi_i^{+} = (2\pi)^{-3/2} \exp(\mathrm{i}\mathbf{K}_i \cdot \mathbf{R}_i)\phi_i(\mathbf{x}) \exp\left(-\mathrm{i}\frac{Z_P}{v} \ln(v\, s - \mathbf{v} \cdot \mathbf{s})\right) \tag{12}$$

where the incident projectile is described by a plane wave and $\phi_i(\mathbf{x})$ is the active electron orbital wavefunction. The multiplicative exponential function in equation (12) denotes an eikonal projectile-electron continuum factor, so that the electron is described simultaneously in the combined fields of the target and the projectile. In this sense, the distorted wavefunction presents intrinsically a two-centre character. The use of two-centre wavefunctions avoids also the possible divergences in the corresponding perturbative series associated with the presence of disconnected diagrams [34].

In the final channel, the *two-effective centre* (TEC) approximation introduced by Wang *et al* [35] (see also Corchs *et al* [23]) to study electron capture by impact of bare ions on homonuclear and heteronuclear molecules has been used. This approximation was then employed by Galassi *et al* [24, 36] to describe single ionization of H_2 molecules by the impact of swift bare ions.

The active electron scattering matrix element is given within this approximation by the following expression,

$$\tilde{T}_{fi}(\boldsymbol{\eta}, \boldsymbol{\rho}) = \tilde{T}_{fi}^{(1)}(\boldsymbol{\eta}) \exp(\mathrm{i}(1 - \mu)\mathbf{q} \cdot \boldsymbol{\rho}) + \tilde{T}_{fi}^{(2)}(\boldsymbol{\eta}) \exp(-\mathrm{i}\mu\mathbf{q} \cdot \boldsymbol{\rho}), \tag{13}$$

where the atomic centres are displaced from the centre of mass of the target by $(1 - \mu)\boldsymbol{\rho}$ for the centre 1 and $\mu\boldsymbol{\rho}$ for the centre 2, $\mu \approx M_1/(M_1 + M_2)$ being the reduced mass, with M_1 and M_2 being the masses of both centres, and $\tilde{T}_{fi}^{(1)}$ and $\tilde{T}_{fi}^{(2)}$ the corresponding effective atomic scattering matrix elements. In equation (13) the exponential phases indicate the Galilean translation factors from the atomic centres to the centre of mass of the molecule.

The CDW-EIS distorted wavefunction in the final channel is thus chosen as

$$\chi_f^{-} = (2\pi)^{-3} \exp\left(\mathrm{i}\mathbf{K}_i \cdot \mathbf{R}_i + \mathrm{i}\mathbf{k} \cdot \mathbf{x}_j\right) N(\gamma)\ {}_1F_1\ (-\mathrm{i}\gamma;\, 1;\, -\mathrm{i}kx_j - \mathrm{i}\mathbf{k} \cdot \mathbf{x}_j) \times N(\zeta)\ {}_1F_1\ (-\mathrm{i}\zeta;\, 1;\, -\mathrm{i}ps - \mathrm{i}\mathbf{p} \cdot \mathbf{s}) \exp(\mathrm{i}\beta_j \mathbf{k} \cdot \boldsymbol{\rho});\quad j = 1 \text{ or } 2, \tag{14}$$

where $\gamma = Z_{\mathrm{eff}}/k$ and $\zeta = Z_P/p$, with $Z_{\mathrm{eff}} = \sqrt{-2\varepsilon_i}$, ε_i being the orbital energy of the active electron. The vectors $\mathbf{k}$ and $\mathbf{p}$ are the active electron momenta with respect to the centre j and to the projectile, respectively. Also, in equation (14), $\beta_1 = 1 - \mu$ and $\beta_2 = -\mu$. The first line in equation (14) describes the dynamics of the projectile as a plane wave. In

addition, the second line defines the wavefunction of the active electron in the field of an effective Coulomb target continuum. Finally the third line includes a Coulomb continuum factor of the electron in the field of the projectile. Thus, the electron is described as moving in the combined fields of the target and the projectile, so that the distorted wavefunction presents also a two-centre character in the final channel. The normalization factors of the target and projectile continuum states are given by the Coulomb factor $N(a) = \exp(\pi a/2)\Gamma(1 + \mathrm{i}a)$ with $a = \gamma$ or $a = \zeta$. According to the TEC approximation, when the electron is emitted from the centre 1 (2), χ_f^- is chosen employing the expression corresponding to $j = 1$ ($j = 2$).

For the case of a homonuclear molecule and after some algebra, it is possible to show that:

$$|\tilde{T}_{fi}(\boldsymbol{\eta}, \boldsymbol{\rho})|^2 = \{1 + \cos[(\mathbf{k} - \mathbf{q}) \cdot \boldsymbol{\rho})]\} \left|\tilde{T}_{fi}^{\mathrm{eff}}(\boldsymbol{\eta})\right|^2, \quad (15)$$

with $\tilde{T}_{fi}^{\mathrm{eff}}(\boldsymbol{\eta}) = \tilde{T}_{fi}^{(1)}(\boldsymbol{\eta}) = \tilde{T}_{fi}^{(2)}(\boldsymbol{\eta})$, an *effective* one-centre scattering T-matrix element. The oscillatory factor in equation (15) is the signature of interferences patterns coming from the electron emission of both effective centres.

For a randomly oriented molecule, equation (15) must be averaged over all molecular orientations, so that

$$|\tilde{T}_{fi}(\boldsymbol{\eta}, \rho)|^2_{\mathrm{avg}} = 4\pi \left[1 + \frac{\sin(|\mathbf{k} - \mathbf{q}|\rho)}{|\mathbf{k} - \mathbf{q}|\rho}\right] \left|\tilde{T}_{fi}^{\mathrm{eff}}(\boldsymbol{\eta})\right|^2. \quad (16)$$

Moreover, DDCS as a function of the final energy and solid angle subtended by the ejected electron, averaged over all molecular orientations, can be obtained by using equations (6) and (16), so that

$$\frac{\mathrm{d}^2\sigma}{\mathrm{d}E_k\,\mathrm{d}\Omega_k} = N_e(2\pi)^4 \frac{4\pi k}{v^2} \int \mathrm{d}\boldsymbol{\eta} \left[1 + \frac{\sin(|\mathbf{k} - \mathbf{q}|\rho)}{|\mathbf{k} - \mathbf{q}|\rho}\right] \left|\tilde{T}_{fi}^{\mathrm{eff}}(\boldsymbol{\eta})\right|^2 = S_{\mathrm{dir}}(E_k, \Omega_k) + S_{\mathrm{int}}(E_k, \Omega_k), \quad (17)$$

$S_{\mathrm{dir}}(E_k, \Omega_k)$ being the contribution to the DDCS given by the effective atomic centre and $S_{\mathrm{int}}(E_k, \Omega_k)$ the interference contribution which corresponds to consider only the oscillatory part of the integrand in equation (17). The relevant physical quantity to observe interference patterns for oriented molecules is the product $(\mathbf{k} - \mathbf{q}) \cdot \boldsymbol{\rho}$. On the other hand, for randomly oriented species it is the factor $|\mathbf{k} - \mathbf{q}|\rho$, the one that governs the interference picture. Moreover, to obtain DDCS we must sum up over all transverse momentum transfers so that depending on the molecular orientation interference patterns may be washed out. Thus, for charged projectiles the condition for the presence of oscillations in the cross sections is not as simple as for photoionization, where, for instance, in randomly oriented molecules the relevant quantity is simply $k\rho$ [38]. For the latter case this condition is given by $k\rho > 1$, which corresponds to an electron with de Broglie's wavelength of the order or smaller than the molecular internuclear distance. One is tempted to assume that for soft electron emission, for which $k, q \ll 1$, no signatures of interference effects will be found. However, according to equations (15) to (17), the fingerprints of coherent electron emission should be observed. Similar situation must be expected when all the momentum q is transferred to the ejected electron ($\mathbf{q} \approx \mathbf{k}$), as in a binary encounter with the projectile. We will come back to the details on these questions throughout the rest of this work.

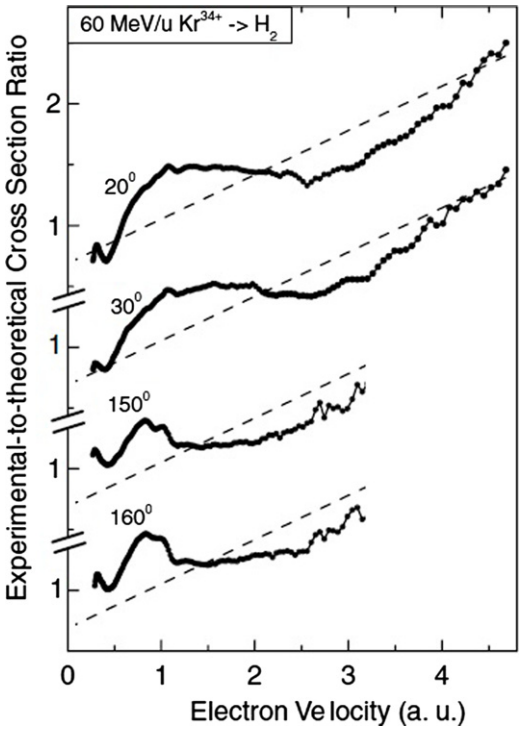

Figure 2. Experimental-to-theoretical cross section ratios for the single ionization of H_2 molecules by 60 MeV amu^{-1} Kr^{34+} projectiles. The electron observation angles are 20°, 30°, 150°, and 160°. The dashed lines are obtained from a linear function introduced to fit the overall increase of the cross section ratios (see text for details).

2.1. The case of dielectronic molecules

As has been previously mentioned, the first experimental evidence on the existence of coherent emission in single ionization by ion impact of dielectronic molecules was given at the beginning of the present century [12]. The doubly differential spectra $\mathrm{d}^2\sigma/\mathrm{d}E_k\,\mathrm{d}\Omega_k$ (DDCS) of electrons emitted from H_2 targets by the impact of 60 MeV amu^{-1} Kr^{34+} ions were measured as a function of the ejected electron energy for fixed observation angles. The experiments were carried out at the GANIL accelerator facility in France. As DDCS decrease strongly by several orders of magnitude with the ejected electron velocity, in order to show the possible presence of coherent emission, experimental DDCS were divided by twice the theoretical DDCS corresponding to *effective hydrogenic* atomic centres with nuclear charge $Z_T = 1.05$ (which follows from the orbital binding energy). Results corresponding to these ratios for polar ejection angles $\theta_e = 20°, 30°, 150°$ and 160° are shown in figure 2. Also, dashed straight lines are introduced to fit the overall cross section ratios and are included to help the view of the undulations. Oscillations associated with interference patterns were thus observed as a clear evidence of coherent electron emission.

In a consecutive work, Galassi *et al* [36], described the initial orbital wavefunction for the hydrogen molecule H_2 by means of a variational single-zeta function

$$\phi_i(\mathbf{x}) = N_i(\rho)\,[\xi(\mathbf{x}_1) + \xi(\mathbf{x}_2)] \quad (18)$$

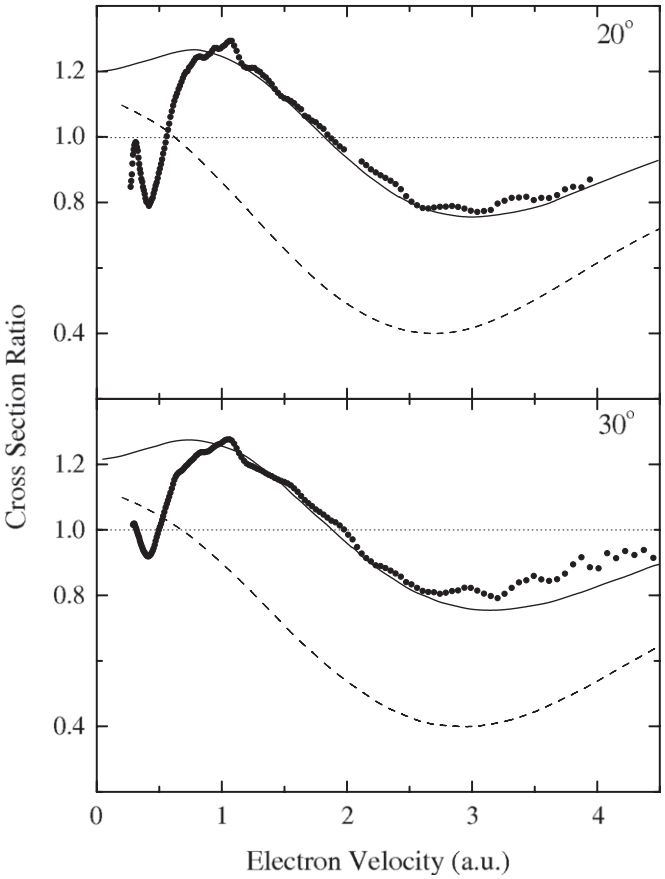

Figure 3. Ratio between the DDCS for single ionization of H_2 and two times the DDCS for ionization of H as a function of electron velocity at 20° and 30° emission angles, for 60 MeV amu^{-1} Kr^{34+} impact. Solid circles: experiment from [12]. Theory: solid line, CDW-EIS calculation [36], dashed line: results of [37].

with

$$\xi(\mathbf{x}_j) = \left(\frac{Z^3}{\pi}\right)^{1/2} \exp(-Zx_j); \qquad j = 1, 2, \tag{19}$$

$Z = 1.193$ and $N_i(\rho) = 0.5459$ being the normalization factor of the wavefunction corresponding to an equilibrium distance $\rho = 1.4$ au. In the calculation of the scattering matrix element $\tilde{T}_{fi}^{\text{eff}}(\boldsymbol{\eta})$, the orbital energy is taken from the experimental value obtained for single ionization of H_2 molecules, i.e. $\varepsilon_i = -0.566$ au. It must be also noted that $N_i(\rho)\xi(\mathbf{x})$ must be considered as an *effective* atomic wavefunction.

In figure 3 the ratio between DDCS for molecular H_2 and twice the atomic H is shown for the mentioned case of impact of 60 MeV amu^{-1} Kr^{34+} projectiles on H_2 targets. The electrons bound to the projectile are considered to be entirely placed onto the corresponding nucleus so that a net charge of $Z_P = 34$ was taken into account in the calculations. The theoretical results are compared with the ones corresponding to divide the measured DDCS by the theoretical ones. The emission in the forward direction for angles of $\theta_e = 20°$ and 30° is considered. The agreement between both resulting curves is excellent for ejection velocities $v_k > 1$ au, even considering that the ratio obtained using the measured data has been divided by the above fitting straight lines to remove its overall increase as the velocity increases (for details see

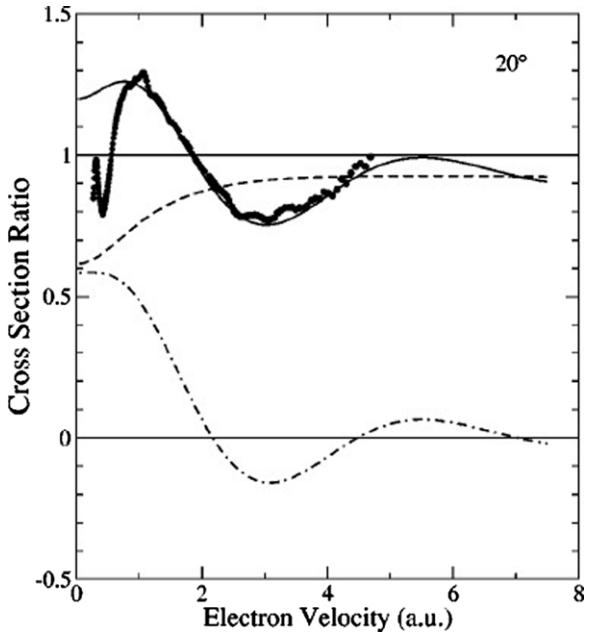

Figure 4. Same as figure 2 at 20° emission angle. Solid circles: experiment from [12]. Theory: solid line, CDW-EIS calculation; dashed-line, contribution from $S_{\text{dir}}(E_k, \Omega_k)$; dot-dashed line, contribution from $S_{\text{int}}(E_k, \Omega_k)$ [36].

Stolterfoht *et al* [12]). Both ratios present characteristics oscillations due to coherent electron emission. They indicate that the integration over all transverse momentum transfer $\boldsymbol{\eta}$ in equation (17) does not wash out completely the oscillatory behaviour. The abrupt fall of the experimental data as the electron energy decreases does not correspond to interference effects but to electron correlation and/or screening effects as it has been shown for photoionization of H_2 targets [39]. These effects are very sensitive to the representation used for the bound and continuum molecular states and are not described by the simple wavefunctions here employed. Calculations using a semiclassical version of a first-order Born peaking approximation [37] are also included for comparison.

In figure 4 contributions to the DDCS ratio from the direct $S_{\text{dir}}(E_k, \Omega_k)$ and interference $S_{\text{int}}(E_k, \Omega_k)$ terms are differentiated for the case of $\theta_e = 20°$ emission angle, for the same collision system. This ratio could be expected to be close to the unity at the high impact energy considered. However, some differences are found due to the different binding energies of H_2 and H, the corresponding effective charges Z_{eff} and the normalization of the respective bound-state wavefunctions. While $S_{\text{dir}}(E_k, \Omega_k)$ increases monotonically, $S_{\text{int}}(E_k, \Omega_k)$ shows a damped oscillatory behaviour with the ejected electron velocity, demonstrating that interference patterns arise from coherent electron emission from the molecular centres.

These works were followed by further experimental investigations proving the existence of coherent electron emission by impact of 68 MeV amu^{-1} Kr^{33+} [40] projectiles and 1, 3 and 5 MeV H^+ [41, 42] projectiles on H_2 molecules. In figure 5, DDCS ratios for 3 MeV H^+ and ejection angles $\theta_e =$ 30° (top panel) and 150° (bottom panel), obtained by dividing the experimental molecular DDCS by twice the atomic H ones, are compared with theoretical predictions (for details see

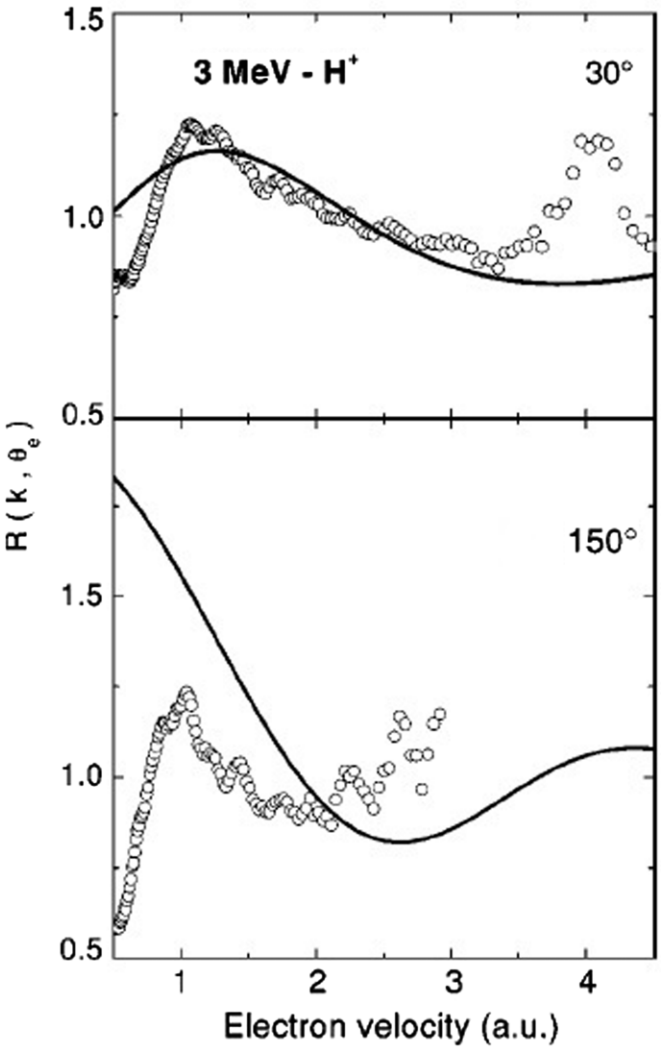

Figure 5. Ratio of the DDCS for electron emission at 30° and 150° from H_2 and 2-H atoms, for 3-MeV proton impact as a function of the ionized electron velocity. Open circles: experiment from [43]. Solid line, CDW-EIS calculation [24].

Galassi *et al* [24]). The qualitative behaviour of experimental data is well reproduced by theoretical calculations (except for $v_k < 1$ au as it has been discussed before). The experimental data [43] for electron velocities larger than 2.5 au must be taken with care considering that, according to [41], the measured cross sections for these velocities are less accurate due to limited statistics. It can be seen that the frequency of the oscillations presented by the ratios depends on the ejection angles. This is an expected result considering that in equation (17), the argument of the oscillatory term in the integrand depends on the emission angle θ_e among other quantities. Moreover, it is easy to show that

$$|\mathbf{k}-\mathbf{q}|^2 = k^2 + k[\eta \sin(\theta_e)\cos(\phi_\eta - \phi_e) + q_{\min}\cos(\theta_e)] + q^2, \tag{20}$$

so that the validity on the utilization of simple analytical forms to describe the interference structures [37, 40] can be questionable as it has been discussed by Galassi *et al* [24]. In equation (20), ϕ_η and ϕ_e are the azimuthal angles of $\boldsymbol{\eta}$ and $\mathbf{k}$, respectively and $q_{\min} = \frac{\Delta\varepsilon}{v_i} = \frac{k^2/2-\varepsilon_i}{v}$ is the minimum momentum transfer, which corresponds to $\eta = 0$.

Additionally, it must be mentioned that second-order oscillations were measured superimposed on the primary oscillatory structure observed in the cross section ratios [42, 44]. The frequency of these oscillations is doubled in comparison with the primary ones and appears to be independent on the emission angle. This effect has been attributed to second-order interferences between electrons emitted directly from each molecular centre with the ones that backscatter at the other centre. However, the difficulty of the procedure employed to obtain the experimental results and the absence of a formal theoretical demonstration on its existence make nowadays the subject a matter of discussion that will be not considered here. Moreover, it has been reported that doubling frequency oscillations are not found in DDCS when a non-perturbative semiclassical approach to solve the TDSE fully numerically is used (see e.g. [30]).

Misra *et al* [45] measured DDCS for the cases of 1.5 MeV amu^{-1} F^{9+} and 1.0 MeV amu^{-1} C^{6+} ions impacting on atomic H and molecular H_2 targets. Cross section ratios were thus obtained by dividing both experimental results and compared with fully theoretical CDW-EIS calculations employing the model introduced by Galassi *et al* [36]. Once again, the presence of interference patterns due to coherent electron emission from the molecular centres was found, confirming the previous results.

In order to avoid the comparison in the cross section ratios between molecular and atomic DDCS, Misra *et al* [46], in the quest for interference patterns in electron emission from H_2, analysed the behavior of the parameter

$$\alpha(k,\theta_e) = \frac{\mathrm{d}^2\sigma/\mathrm{d}E_k\,\mathrm{d}\Omega_k(k,\theta_e) - \mathrm{d}^2\sigma/\mathrm{d}E_k\,\mathrm{d}\Omega_k(k,\pi-\theta_e)}{\mathrm{d}^2\sigma/\mathrm{d}E_k\,\mathrm{d}\Omega_k(k,\theta_e) + \mathrm{d}^2\sigma/\mathrm{d}E_k\,\mathrm{d}\Omega_k(k,\pi-\theta_e)} \tag{21}$$

involving only molecular results. This α parameter, which accounts for the forward–backward asymmetry in electron emission, was measured for the case of 80 MeV C^{+6} (see also [49] for 6 MeV amu^{-1} C^{6+}) projectiles. Oscillations characteristics of interference patterns were clearly found superimposed with an increase of the α parameter with the electron velocity, the latter associated with the well known *two-centre projectile-residual target effect* showing that the electron has the preference to be emitted in the forward direction due to the attractive action of the projectile field [19, 48].

Furthermore, in order to investigate the influence of the molecular orientation on the interference patterns, the triply differential cross section (TDCS), which results from introducing equation (15) in equation (6), was evaluated for the impact of 13.7 MeV amu^{-1} C^{6+} projectiles on H_2 [47]. A full coplanar geometry, where the molecule, the emitted electron and the projectile velocity are all in the same plane, is considered. An integration on the transverse momentum transfer $\boldsymbol{\eta}$ is necessary in order to obtain the corresponding cross sections. Angular distributions are shown in figure 6 for a 100 eV fixed ejection electron energy, as a function of the emission angle for different molecular orientations.

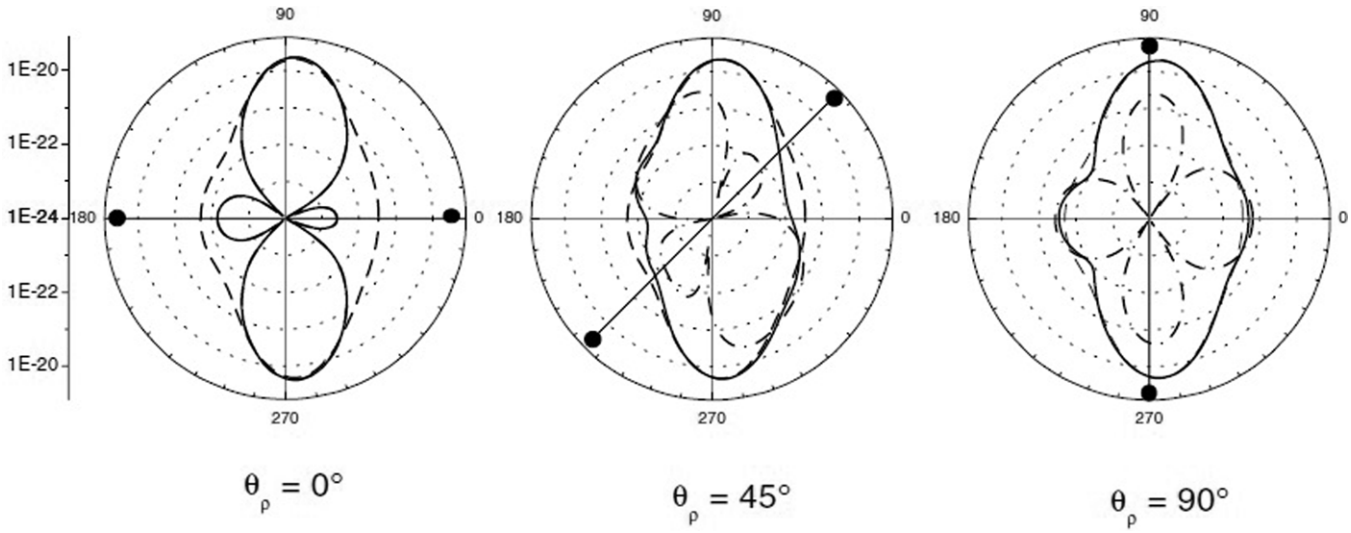

Figure 6. Angular distribution of emitted electrons at 100 eV for different orientations of the H_2 molecule, $\theta_\rho = 0°$, 45° and 90°. All curves present theoretical CDW-EIS calculations. Full curve, full molecular calculation; chain curve, molecular calculation but neglecting the contribution of $\boldsymbol{\eta}$ to the interference factor (see text); dashed curve, results for two-*effective* H atoms.

For a molecular orientation parallel to the impact velocity, $\boldsymbol{\eta}$ is perpendicular to $\boldsymbol{\rho}$ and does not contribute to the interference factor (see equation (15)), in such a way that

$$|\tilde{T}_{fi}(\boldsymbol{\eta}, \boldsymbol{\rho})|^2 = \left\{1 + \cos\left[\mathbf{k}\cdot\boldsymbol{\rho} - \frac{\Delta\varepsilon}{v}\rho\right]\right\}\left|\tilde{T}_{fi}^{\mathrm{eff}}(\boldsymbol{\eta})\right|^2, \quad (22)$$

and the only dependence on $\boldsymbol{\eta}$ is contained in the term $\left|\tilde{T}_{fi}^{\mathrm{eff}}(\boldsymbol{\eta})\right|^2$. Thus, the corresponding oscillatory behaviour observed in figure 6 is dominated by the interference factor in equation (22), showing four lobes with a predominance of electron emission in the direction perpendicular to the initial projectile velocity. For the electron energy here considered $k\rho \approx 3.8$, which corresponds to a de Broglie's wavelength $\lambda = 2.31$ au, satisfying thus the condition $k\rho > 1$. As the orientation is modified from this position, different $\boldsymbol{\eta}$ contribute to the interference factor and thus to the calculation of the TDCS, tending to wash out the presence of interferences (see equations (6) and (15)). To give further support to this analysis, cross sections calculated neglecting the contribution of $\boldsymbol{\eta}$ in the interference factor are also shown in figure 6 for different molecular orientations. In all the cases, characteristics of four interference lobes appear with a preference of electrons to be emitted in the direction perpendicular to the molecular orientation. Results corresponding to the case of two-effective atoms, obtained by neglecting completely the interference factor (replacing it by the unity, as if the atoms were not separated one of the other), are also included. At the ejected electron energy considered the emission appears to be preferable in the direction perpendicular to the impact projectile velocity.

Fully differential cross sections (FDCS) given by equation (4) were theoretically computed for impact of 6 MeV protons on H_2 molecules [50]. According to equations (1) and (2), the interaction between the projectile and the residual target must be included in the calculations [51]. Following the procedure given in [24], it can be shown that the structures of these FDCS are dominated by the ones present in the interference factor

$$F^{\theta_\rho,(\theta_e,\phi_e)}(\mathbf{k}, \mathbf{q}, \boldsymbol{\rho}) = \{1 + \cos[(\mathbf{k} - \mathbf{q})\cdot\boldsymbol{\rho}]\} \quad (23)$$

with θ_ρ the polar angle that gives the orientation of the molecule with respect to the projectile impact velocity direction, i.e. the z-axis. Considering that the molecular axis lies in the collision plane, the argument of the oscillatory term in equation (23) can be written in spherical coordinates as

$$(\mathbf{k}-\mathbf{q})\cdot\boldsymbol{\rho} = (k\sin\theta_e\cos\phi_e + q, k\sin\theta_e\sin\phi_e, k\sin\theta_e + q_{\min}) \cdot (\rho\sin\theta_\rho, 0, \rho\cos\theta_\rho). \quad (24)$$

In figures 7 and 8, FDCS are represented as a function of θ_e for the H_2 molecule aligned parallel ($\theta_\rho = 0$) or perpendicular ($\theta_\rho = \pi/2$) to the projectile impact velocity. From both figures we can observe the most important structures that appear in the in-plane FDCS for single ionization for high enough impact velocities: the binary and recoil peaks. The former, located at $\theta_e \approx \pi/2$ and $\phi_e = \pi$, emerges as a consequence of a binary collision between the projectile and the active electron. On the other hand, the latter, that arises at $\theta_e \approx \pi/2$ and $\phi_e = 0$, is a consequence of a two-step process: first the projectile collides with the active electron and after that the electron interacts with the residual nuclear target ion.

Different kinematical conditions are analysed corresponding to $E_k = 10$ eV and $q = 0.5$ au or $q = 0.8$ au and $E_k = 30$ eV for similar momentum transfers. For molecular parallel alignment, the typical binary and recoil peaks appear as a consequence of partial constructive interferences, according to equation (23). However, for molecular perpendicular alignment, signatures of partial destructive interferences are found in the recoil peak region. It has been shown that this effect appears to be less pronounced as the cross sections are averaged over all molecular orientations [50]. The above mentioned theoretical predictions require an ensemble of highly oriented molecules in order to be observed. In laser-matter physics, studies of laser induced processes with aligned and oriented molecules

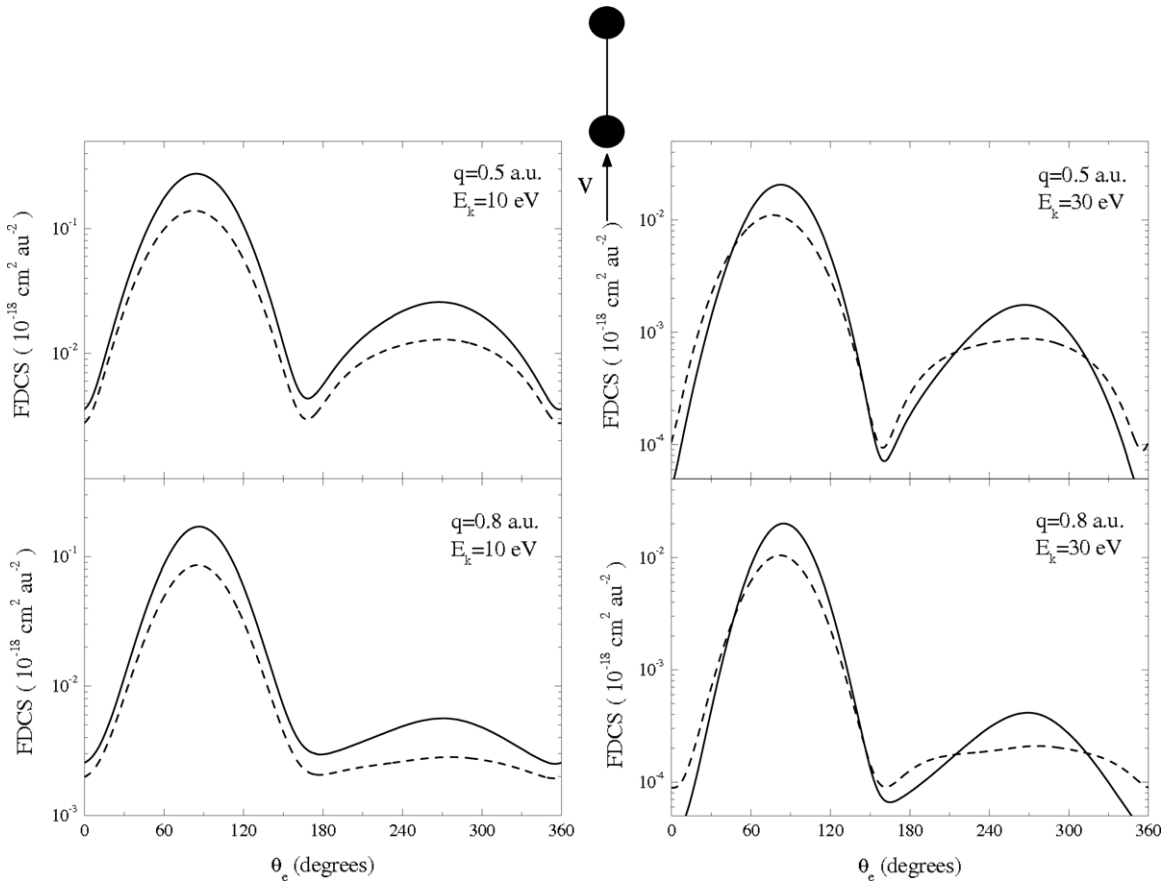

Figure 7. FDCS for single ionization of H_2 molecules by impact of 6 MeV protons. The H_2 molecule is aligned parallel with respect to the beam direction ($\theta_\rho = 0$). Solid line: total contribution, dashed line: direct contribution.

have reached high maturity (for one of the most prominent and interesting examples see e.g. [52]) and consequently we consider plausible to use similar techniques, combined with projectile beams, to produce experimental results to be compared with our theoretical outcomes. It has been demonstrated experimentally that molecules in gas-phase can be aligned adiabatically [53] or non-adiabatically [54, 55], aligned in three dimensions [56] or oriented [57]. All these schemes appear to be suitable in order to prepare the molecular targets before the interaction with the charged projectiles. There could exist, however, complications with the synchronization between the laser and the projectile beam that should be solved.

Alexander *et al* [58] have measured DDCS $\mathrm{d}^2\sigma/\mathrm{d}E_k\,\mathrm{d}\Omega_s$ as a function of the projectile scattering angle θ_s for fixed projectile energy losses. The case of 75 keV protons impacting on H_2 targets and energy losses ranging from 30 to 70 eV were considered. Oscillatory structures found at large enough θ_s scattering angles were in good agreement with the CDW-EIS predictions. On the contrary, when replacing the molecular target by He atomic targets, under similar kinematical conditions, cross sections showed a monotonically decreasing behaviour as θ_s increases without the presence of undulations. In order to further investigate the role played by the molecular orientation on coherent electron emission, $\mathrm{d}^2\sigma/\mathrm{d}E_k\,\mathrm{d}\Omega_s$ ratios between the experimental data and theoretical calculations for two H atoms were obtained (see figure 9). With such a goal in mind, the orientation of the molecular target was experimentally estimated as a function of the projectile polar angle. This estimation suggested that for small scattering angles a transverse molecular orientation dominates while for large scattering angles a parallel orientation mostly contributes, this result being qualitatively valid for every energy loss. Cross section ratios appear to be more sensitive than total cross sections to the molecular orientation. According with equations (1)–(3), the cross sections depending on Ω_s, i.e., depending on the projectile scattering angles, must be influenced by the interactions of the projectile with the target nuclei and passive electrons. It is clear, for instance, that a change on the position of the target nuclei will affect the projectile trajectory. Two different CDW-EIS calculations were thus done. The first one employs the T-matrix element given by equation (16) and in the second one the measured dependence of the molecular orientation with the projectile scattering angle was included. In fact, an average on molecular orientation was not done but on the contrary a particular orientation was assigned to each projectile scattering angle according to the measured data. In the second case, the CDW-EIS calculations largely improve the agreement between the experiments and theoretical estimations. In a recent work using the M3DW-EIS model [28], it has been shown that a qualitative agreement with the measured interference structures was also obtained without assuming that molecular orientations are favoured

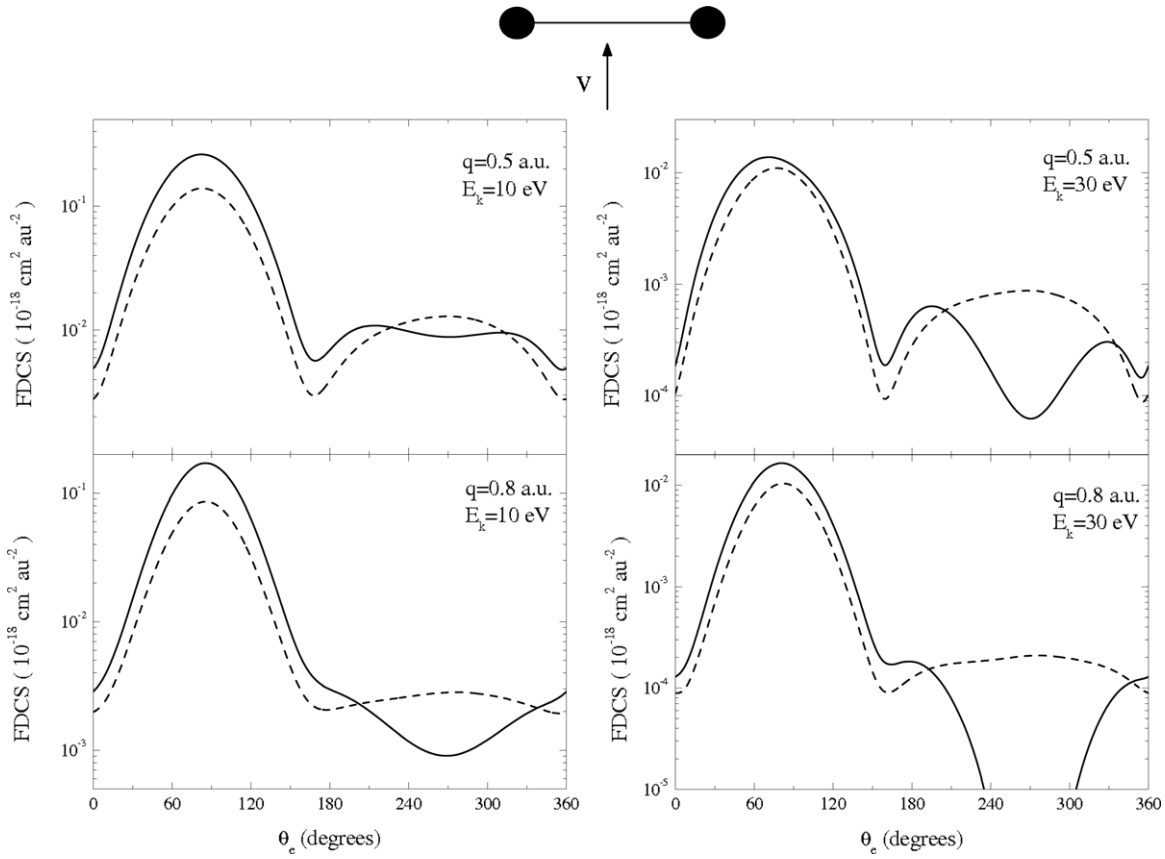

Figure 8. FDCS for single ionization of H_2 molecules by impact of 6 MeV protons. The H_2 molecule is aligned perpendicular with respect to the beam direction ($\theta_\rho = \pi/2$). Solid line: total contribution, dashed line: direct contribution.

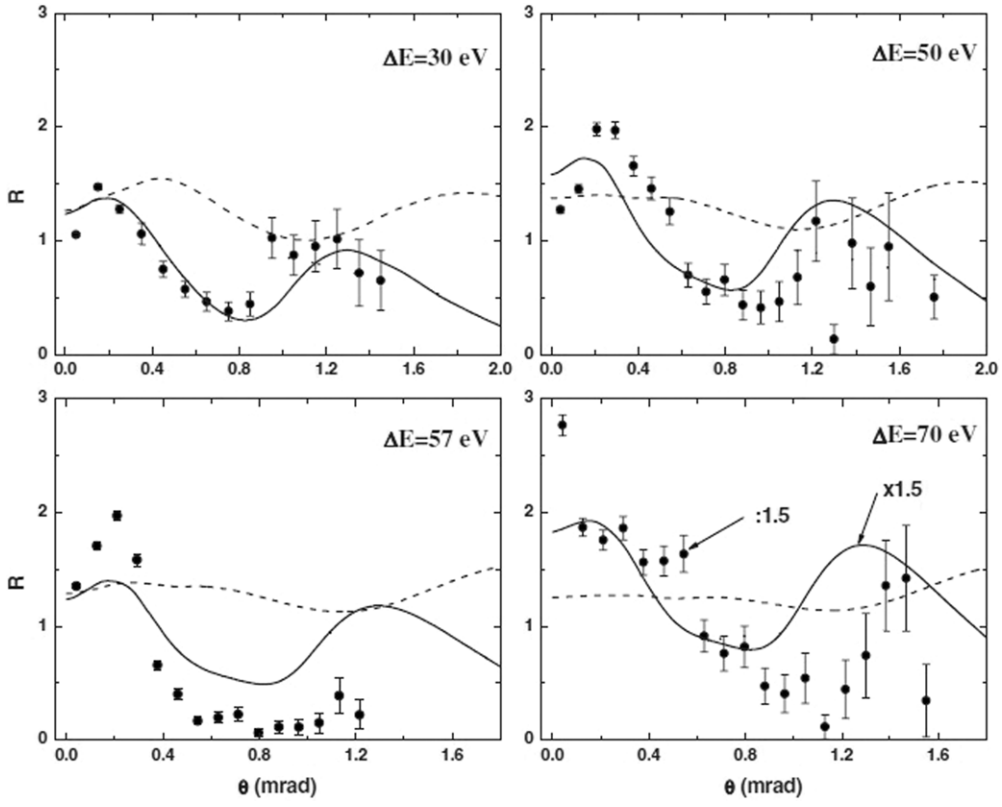

Figure 9. Ratios between measured DDCSs for H_2 and twice the theoretical DDCSs for atomic hydrogen for energy losses of 30, 50, 57, and 70 eV. Dashed curves: CDW-EIS calculation; and solid curves: CDW-EIS calculation with fixed molecular orientation (for details see [58]).

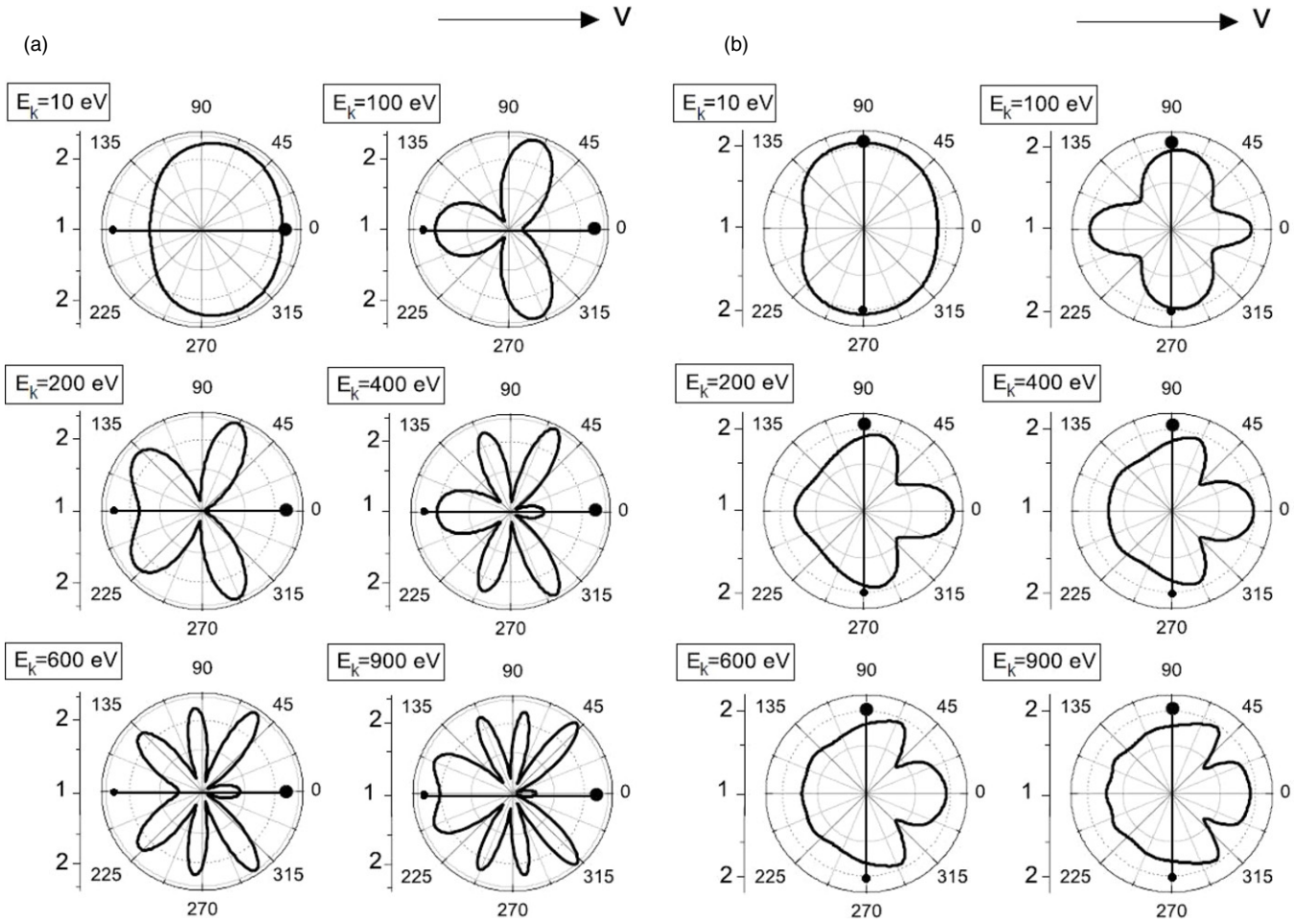

Figure 10. Triple-fold differential cross section ratios for single ionization of HeH^+ by impact of 1 MeV protons: (a) parallel orientation ($\theta_\rho = 0^\circ$) and (b) perpendicular orientation ($\theta_\rho = 90^\circ$) of the molecule with respect to the ion beam [61].

at specific projectile scattering angles. Moreover, in a recent work it was shown that the preparation of the incident beam in the case of ion impact may play an important role on the experimental observation of signatures of interference patterns in differential cross sections measured as a function of the projectile scattering angle at fixed projectile energy loss (see e.g. [59]).

Highly differential cross sections for dissociative single ionization of H_2 molecules by 6 MeV proton impact have been measured using COLTRIMS [60]. The few-particle dynamics is fully determined from the momentum balance of all the fragments and, within the axial recoil approximation, molecular-frame angular distributions of the emitted electrons have been determined for molecules oriented perpendicular to the projectile beam. The experimental data is compared with the CDW-EIS theory, which is able to predict electron emission characteristics for non-dissociative ionization of the H_2 molecule as a function of the orientation of the molecular axis.

The possibility of the presence of coherent electron emission in the case of dielectronic heteronuclear molecules by impact of bare ions was investigated by Tachino *et al* [61–63]. The HeH^+ ion target was considered, which is the only bound diatomic molecule composed by a proton and a helium atom. This is a highly asymmetric system where the electrons have a large preference to be placed in the proximities of the alpha particle in the molecular initial orbital. A Hartree–Fock approximation is used to describe the ground state of the molecule, where both electrons occupy the 1σ orbital, $\psi_i(\mathbf{x})$, one with spin up and the other with spin down. This orbital is described by a minimal basis set of Slater-type orbitals (STO) centred on each molecular nucleus:

$$\psi_i(\mathbf{x}) = \omega_1 \phi_1^{\mathrm{STO}}(\mathbf{x}_1) + \omega_2 \phi_2^{\mathrm{STO}}(\mathbf{x}_2), \qquad (25)$$

where the subscripts 1 and 2 denote the He^{2+} and H^+ nuclei, respectively. The exponents of the STO functions (which correspond to 1s atomic orbitals) and the coefficients ω_j (with $j = 1, 2$) were variationally optimized by employing the quantum chemistry program Gaussian 98 [66]. These quantities were calculated by using a STO-6G basis set within the Hartree–Fock approximation, with each STO function described as a linear combination of six Gaussian-type orbitals [64, 65]. Although the minimal linear combination of atomic orbitals (LCAO) description is appropriate to evaluate transition amplitudes, more accurate values of the corresponding orbital energy ε_i and of the equilibrium internuclear molecular distance ρ appear to be necessary [61]. Thus, they are calculated using a much larger 6-311 G* basis set, so that $\varepsilon_i = -1.63317$ au and $\rho = 0.771$ Å (1.46 au).

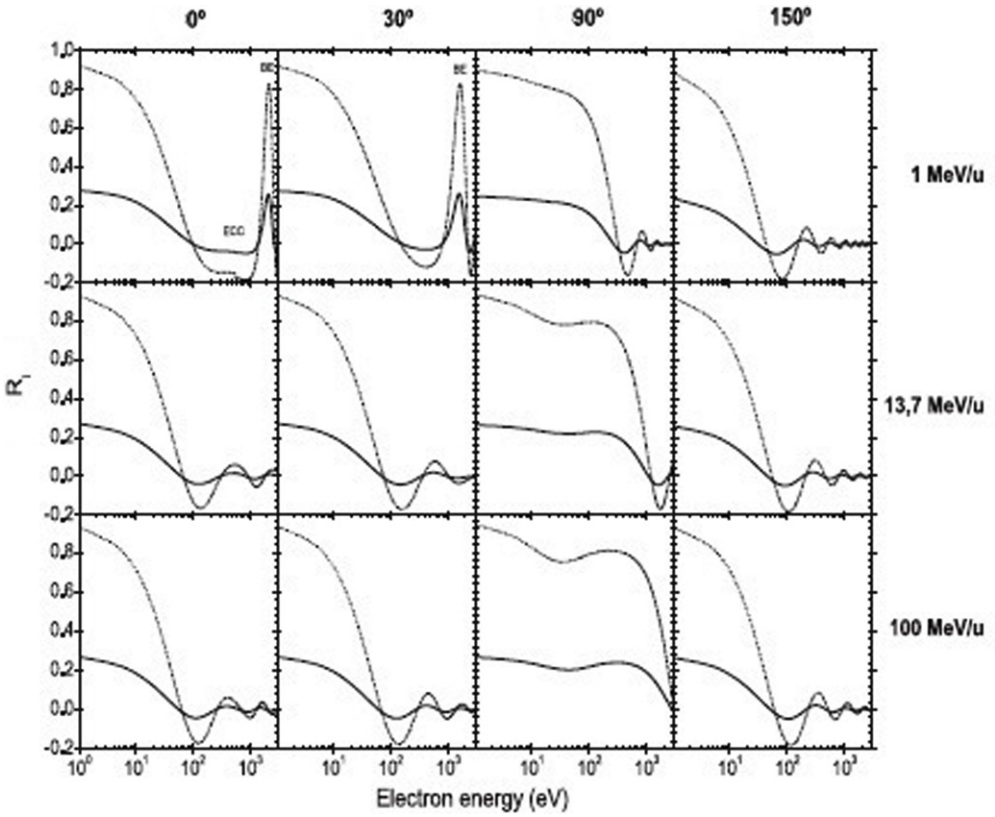

Figure 11. Comparison between the cross section ratios for single ionization of HeH^+ by proton impact. Solid lines R_{i,HeH^+} and dot-dashed lines R_{i,H_2} for different impact energies and different values of θ_e. ECC and BE denote the electron capture to the continuum and binary encounter regions, respectively [62].

Triply differential cross section (TDCS) ratios corresponding to the case of a fully coplanar geometry, where the molecule, the emitted electron and the projectile velocity are in the same plane, are shown in figure 10 for single ionization of HeH^+ by impact of 1 MeV protons. For this asymmetric case, the ratios were defined as the ones obtained by dividing the molecular TDCS $d^3\sigma/dE_k\ d\Omega_k\ d\Omega_\rho$ by twice the effective atomic DDCS corresponding to the $\omega_1\phi_1^{STO}$ term of the MO (this is the term describing the dominant molecular distribution of the electron around the alpha particle). Two molecular orientations were considered, parallel and perpendicular to the impact projectile velocity. The ratios are presented for fixed ejection electron energies ranging from 10 to 900 eV as a function of the electron emission angle in the different panels of figure 10. For parallel orientation (i.e. for $\boldsymbol{\eta}\cdot\boldsymbol{\rho}=0$), the interference factor does not depends on the transverse momentum transfer (see equation (22)), as it happens for H_2 targets, and thus is not affected by the integration needed to calculate TDCS (see equation (6)). The number of lobes associated with interference patterns increases as the ejection electron velocity increases. For perpendicular orientation, on the contrary, the transverse momentum transfer in the interference factor contributes to the determination of the TDCS, so that structures characteristics of coherence are washed out.

For the asymmetric target case here considered, the DDCS can be written under the form

$$\begin{aligned}\frac{d^2\sigma}{dE_k\,d\Omega_k}&=N_e(2\pi)^4\frac{4\pi k}{v^2}\left[\omega_1^2\int d\boldsymbol{\eta}|\tilde{T}_{fi}^{(1)}(\boldsymbol{\eta})|^2+\omega_2^2\int d\boldsymbol{\eta}|\tilde{T}_{fi}^{(2)}(\boldsymbol{\eta})|^2\right]\\&+N_e(2\pi)^4\frac{4\pi k}{v^2}\omega_1\omega_2\int d\boldsymbol{\eta}\frac{\sin(|\mathbf{k}-\mathbf{q}|\rho)}{|\mathbf{k}-\mathbf{q}|\rho}\left[\tilde{T}_{fi}^{(1)}(\boldsymbol{\eta})\left(\tilde{T}_{fi}^{(2)}(\boldsymbol{\eta})\right)^*\right.\\&\left.+\left(\tilde{T}_{fi}^{(1)}(\boldsymbol{\eta})\right)^*\tilde{T}_{fi}^{(2)}(\boldsymbol{\eta})\right]\\&=S_{dir}^{(1)}(E_k,\Omega_k)+S_{dir}^{(2)}(E_k,\Omega_k)+S_{int}(E_k,\Omega_k)\end{aligned}\tag{26}$$

where the first and second terms, i.e. $S_{dir}^{(1)}(E_k,\Omega_k)$ and $S_{dir}^{(2)}(E_k,\Omega_k)$, correspond to the direct contributions from the electronic distribution around the molecular centres 1 and 2 while the third one, $S_{int}(E_k,\Omega_k)$, gives the interference one.

The following cross section ratio

$$\begin{aligned}R(E_k,\Omega_k)&=1+\frac{S_{int}(E_k,\Omega_k)}{S_{dir}^{(1)}(E_k,\Omega_k)+S_{dir}^{(2)}(E_k,\Omega_k)}\\&=1+R_i(E_k,\Omega_k),\end{aligned}\tag{27}$$

is defined in order to investigate how the partial localization of the electron around the alpha particle influences the oscillatory behaviour due to coherent electron emission from both molecular centres. In figure 11 the ratios $R_i(E_k,\Omega_k)$ given by equation (27) are shown as a function of the final electron energy at fixed ejection angles. The case of protons as projectiles with impact energies ranging from 1 to 100 MeV

is considered. Interference patterns appear under the form of smooth oscillations with the property that for a fixed collision energy the ratio frequency is larger for backward scattering in comparison with the forward one, as it was previously observed for H_2 targets.

For comparison, the case of H_2 targets is also considered. The corresponding interference term will be now given by $R_{i,H_2}(E_k, \Omega_k) = S_{\mathrm{int},H_2}(E_k, \Omega_k)/2S_{\mathrm{dir},H}(E_k, \Omega_k)$. It is shown that oscillations are in good agreement with the ones corresponding to HeH^+, but with larger amplitudes. This strong reduction in the amplitudes for HeH^+ has been attributed to the partial localization of the electron around one of the molecular centres. A recent investigation using a first-order version of the Born approximation has confirmed these preceding results [67].

It should be also noted that the pronounced peaks in the binary encounter region, shown in figure 11 for 1 MeV protons impact (top row) on H_2 targets at $\theta_e = 0^\circ$ and $\theta_e = 30^\circ$, come from partial constructive interferences. This affirmation can be supported by the fact that in this region, the condition $\mathbf{k} \approx \mathbf{q}$ must be satisfied, so that $\sin(|\mathbf{k}-\mathbf{q}|\rho)/|\mathbf{k}-\mathbf{q}|\rho \approx 1$ in equation (16). The same behaviour is observed at low ejection electron energies for all emission angles, where $q \ll k \ll 1$ and again partial constructive interferences are observed.

2.2. Multi-orbital diatomic targets

Let us consider in the following the case of diatomic molecules composed by a few electron orbitals. In order to describe its initial fundamental state the corresponding wavefunctions are written as linear combinations of STOs centred on each one of the nuclei of the molecule. As it has been previously considered for the one-orbital molecules, the optimization of the linear coefficients and the STO-exponents was done by using the program Gaussian 98 [66], where each STO is written as a combination of Gaussian-type orbitals by employing a minimal STO-6G basis set. The equilibrium distance ρ and the orbital energies ε_i were then calculated with a higher precision by means of the larger HF/6-311 G* basis set.

At first, we focus our interest on collisions between fast protons and N_2 targets initially in its fundamental state $^1\Sigma_g^+$. In this case, σ-MOs are described by linear combinations of 1s, 2s and $2p_z$ STO, whereas π-ones are represented as linear combinations of $2p_x$ and $2p_y$ STO, being the z-axis coinciding in direction with the internuclear molecular vector (for details see [68]). As it has been done before the TEC approximation is employed, where Coulomb continuum states are considered in the final channel, centred on each molecular nuclei. The scattering matrix element $T_{fi,MO}(\boldsymbol{\eta}, \boldsymbol{\rho})$ per electron for each MO can be written as a linear combination of effective one-centre scattering matrix elements $T^{\mathrm{eff}}_{h,MO}(\boldsymbol{\eta}, \boldsymbol{\rho})$ associated with a basis of STO centred on the h-target nucleus, given by

$$T^{\mathrm{eff}}_{h,MO}(\boldsymbol{\eta}, \boldsymbol{\rho}) = \sum_j \omega_{h,j} T^{\mathrm{eff}}_{hj,MO}(\boldsymbol{\eta}, \boldsymbol{\rho}) \tag{28}$$

where $h = 1, 2$ identifies the nucleus of the molecules in which the STO is centred and the subscript j denotes the corresponding quantum numbers nlm. The square modulus of $T_{fi,MO}(\boldsymbol{\eta}, \boldsymbol{\rho})$ can then be written as

$$\begin{aligned}|T_{fi,MO}(\boldsymbol{\eta}, \boldsymbol{\rho})|^2 = &\sum_h |T^{\mathrm{eff}}_{h,MO}(\boldsymbol{\eta}, \boldsymbol{\rho})|^2 \\ &+ \cos[(\mathbf{k}-\mathbf{q})\cdot\boldsymbol{\rho}]\left[(T^{\mathrm{eff}}_{1,MO}(\boldsymbol{\eta}, \boldsymbol{\rho}))^* T^{\mathrm{eff}}_{2,MO}(\boldsymbol{\eta}, \boldsymbol{\rho})\right. \\ &\left. + T^{\mathrm{eff}}_{1,MO}(\boldsymbol{\eta}, \boldsymbol{\rho})(T^{\mathrm{eff}}_{2,MO}(\boldsymbol{\eta}, \boldsymbol{\rho}))^*\right] \\ &-2\mathrm{i}\sin[(\mathbf{k}-\mathbf{q})\cdot\boldsymbol{\rho}]\left[(T^{\mathrm{eff}}_{1,MO}(\boldsymbol{\eta}, \boldsymbol{\rho}))^* T^{\mathrm{eff}}_{2,MO}(\boldsymbol{\eta}, \boldsymbol{\rho})\right. \\ &\left. - T^{\mathrm{eff}}_{1,MO}(\boldsymbol{\eta}, \boldsymbol{\rho})(T^{\mathrm{eff}}_{2,MO}(\boldsymbol{\eta}, \boldsymbol{\rho}))^*\right]. \end{aligned} \tag{29}$$

The TDCS for the complete molecule can be obtained by integrating equation (29) on the transverse momentum transfer for every molecular orbital (MO) and adding all these partial contributions up:

$$\begin{aligned}\frac{\mathrm{d}^3\sigma}{\mathrm{d}E_k\,\mathrm{d}\Omega_k\,\mathrm{d}\Omega_\rho} &= \sum_{MO}\left(\frac{\mathrm{d}^3\sigma}{\mathrm{d}E_k\,\mathrm{d}\Omega_k\,\mathrm{d}\Omega_\rho}\right)_{MO} \\ &= \sum_{MO} N_{MO}(2\pi)^4\frac{k}{v^2}\int \mathrm{d}\boldsymbol{\eta}|T_{fi,MO}(\boldsymbol{\eta}, \boldsymbol{\rho})|^2, \end{aligned} \tag{30}$$

with N_{MO} the occupancy number corresponding to each orbital. DDCS are then calculated averaging equation (30) over all possible molecular orientations.

TDCS for impact of 1 MeV protons on N_2 molecules are presented in figure 12. Contributions from each MO are discriminated for a full coplanar geometry. Two molecular orientations, parallel and perpendicular to the initial collision velocity, and an ejection electron energy of 100 eV, are considered. The lobes present for parallel orientation give evidence of the presence of interference patterns. On the contrary, for perpendicular orientation the contribution of different transverse momentum transfer washes out the signature of coherent electron emission, as it was before observed for H_2 targets. It must be noted that for parallel orientation the phase of the structures is shifted with respect to the others depending on the orbital considered. As a consequence, it has been verified by Tachino *et al* [68] that the TDCS for the complete molecule do not present oscillations associated with interference effects. It explains the suppression of primary electron interferences in the experiments of Baran *et al* [69, 70] where DDCS were measured for impact of proton beams with N_2 molecules. They suggest that this suppression could come from the delocalization of several MOs. Winkworth *et al* [71, 72] have obtained a similar behaviour for impact of H^+ and $O^{5+,8+}$ projectile beams on O_2 targets.

In figure 13, we show ratios for impact of 1 and 3 MeV protons on N_2 molecules. They are obtained by dividing the experimental and theoretical DDCS for the complete molecule with the theoretical ones corresponding to two atomic nitrogen atoms as a function of the electron emission energy at fixed ejection angles of 30°, 45° and 60°. No evidence of interference patterns are found.

It should be also mentioned that, when theoretical DDCS for electron emission from the $1s\sigma_g$ and $1s\sigma_u^*$ inner orbitals are divided by the ones obtained by neglecting the oscillatory terms in equation (29), it was shown that the corresponding ratios are in phase opposition. This behaviour has been explained by the fact that the initial wavefunctions of these

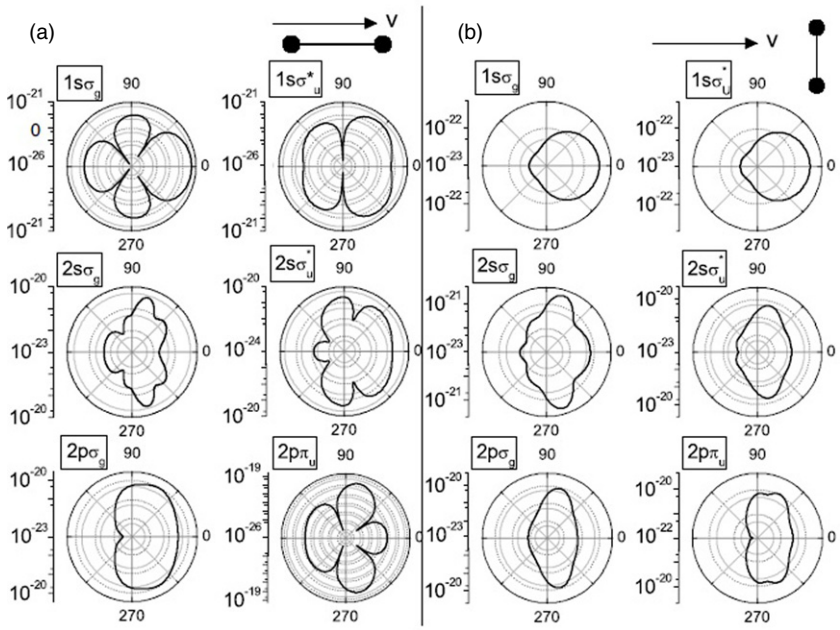

Figure 12. TDCS for each orbital of the N_2 molecule as a function of the emission angle θ_e and for a final electron energy $E_k = 100$ eV, for a molecule aligned (a) parallel and (b) perpendicular to the direction of the incoming projectile. The energy of the incident proton is 1 MeV. TDCS are given in eV^{-1} sr^{-2} cm^2 [68].

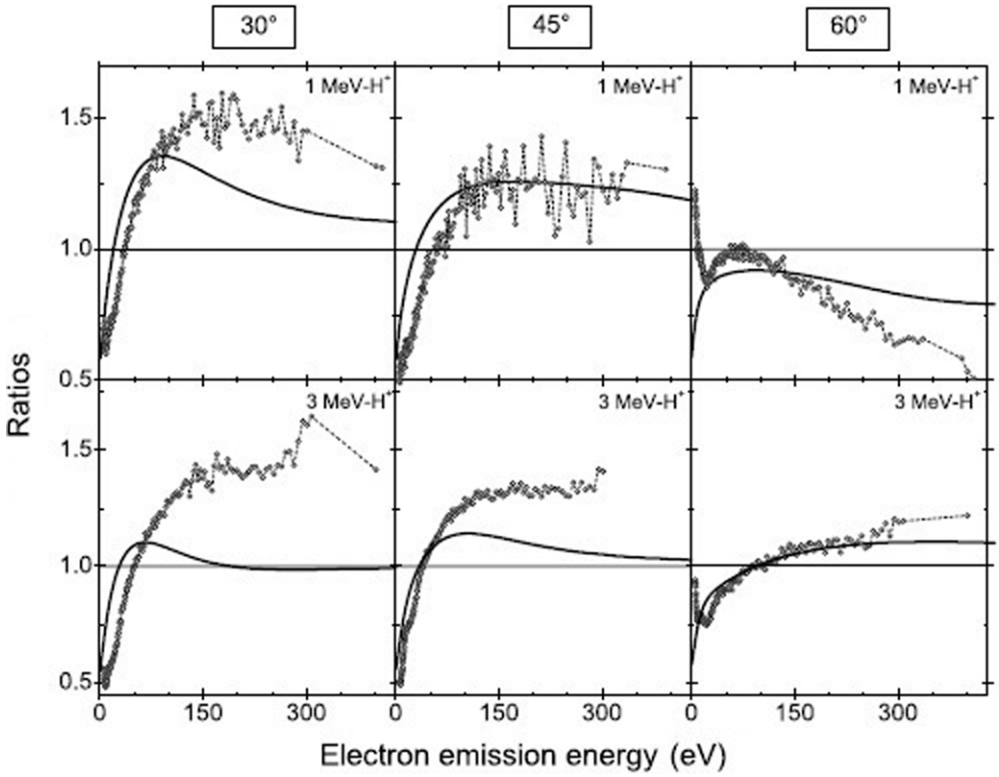

Figure 13. Theoretical (solid line) and experimental (open circles) DDCS ratios corresponding to impact of protons at 1 and 3 MeV on N_2 molecules. Experimental Auger structures have been eliminated for a better comparison with the theory [68].

almost degenerate orbitals, i.e.

$$\phi_{i,\sigma_g^{1s}}(\mathbf{x}) = \omega_{1s}\phi_{1s}^{STO}(\mathbf{x}_1) + \omega_{1s}\phi_{1s}^{STO}(\mathbf{x}_2) \quad (31)$$

$$\phi_{i,\sigma_u^{1s}}(\mathbf{x}) = \omega_{1s}\phi_{1s}^{STO}(\mathbf{x}_1) - \omega_{1s}\phi_{1s}^{STO}(\mathbf{x}_2), \quad (32)$$

present different (gerade or ungerade) symmetries.

Furthermore, Baran *et al* [70] and later Winkworth *et al* [71] reported the presence of secondary interference oscillations (doubling frequency) in DDCS ratios for the cases of nitrogen (N_2) and oxygen (O_2) molecular targets. However, no formal evidence of their existence has been given. The comments expressed earlier for hydrogen molecules can be also extended for these more complex molecular species. Recent experimental and theoretical investigations for impact of fast bare carbon ions on O_2 molecules confirm that neither

primary nor secondary interference effects appear when DDCS for the complete molecular target are considered [73, 74].

3. Electron beam projectiles

Let us consider now the ionization of molecules interacting with electron beams. The dynamics associated to electron impact collisions is quite different in some aspects from the one resulting from heavy-ion impact since electrons are dimensionless, negatively charged and have light mass with larger de Broglie's wavelengths at identical velocities. However, similarities may also appear in the basic physics underlying some phenomena. In particular, we give in the following the main features found in the search of evidence for the coherent electron emission from simple molecules interacting with electrons and we compare them with the heavy-ion impact case.

3.1. First-order models

The reaction of interest is the single ionization of diatomic molecules in their ground state by electron impact. As a benchmark for theoretical developments, we consider in the following the case of ground state H_2 molecular targets for which the single ionization by electron impact reaction reads,

$$e^- + H_2(^1\Sigma_g^+) \rightarrow 2e^- + H_2^+. \tag{33}$$

The ionization process may be considered as a pure electronic transition by applying closure relations over all possible final rotational and vibrational states of the residual molecular target [75, 76]. At the energies involved in this section, the effective collision time is much smaller than the rotational and vibrational ones, therefore the internuclear molecular vector can be considered as frozen during the whole reaction. As a consequence, only vertical transitions at the equilibrium distance from the $^1\Sigma_g^+$ ground state of the molecular target to the specific final electronic state of the H_2^+ molecule are assumed. We consider asymmetric kinematics conditions where a slow and a fast electron are detected in the final channel of the reaction. Under these conditions, exchange effects may be safely disregarded.

Different from heavy ions as projectiles, no semiclassical approximation may be invoked for the trajectory of the incident electron due to the fact that its de Broglie's wavelength is not negligible and a full quantum mechanical treatment must be employed. In this way, several theoretical models, some of them including higher order effects, have been developed to study ionization of atoms and molecules by electron impact (see for instance [77] and the references therein). However, in the context of coherent electron emission from molecules, most of the progress was obtained through the use of first-order models. Therefore, in this subsection we restrict ourselves to the description of them. As a consequence, the T-matrix element for the reaction of interest is given in its *prior* form by,

$$T_{fi}^- = \langle \Psi_f^- | V_i | \psi_i \rangle \tag{34}$$

where Ψ_f^- represents the exact final wavefunction satisfying incoming final asymptotic boundary conditions, ψ_i is the non-perturbed electronic wavefunction in the initial channel of the reaction and V_i is the associated perturbation. Equation (34) is closely related to equation (8) for heavy projectiles but here the notation $\langle\cdot\rangle$ indicates integration over a pair of Jacobi coordinates.

The observables of the reaction, i.e., FDCS per orbital, are obtained as,

$$\frac{d^6\sigma}{d\Omega_\rho\, d\Omega_k\, d\Omega_s\, d(k^2/2)} \cong N_e (2\pi)^4 \frac{kK_f}{K_i} |T_{fi}^-(\boldsymbol{\rho})|^2 \delta(E_f - E_i), \tag{35}$$

where K_i, k and K_f denote the magnitudes of $\mathbf{K}_i$, $\mathbf{k}$ and $\mathbf{K}_f$, i.e., the incident, ejected and scattered electron momenta, respectively. Ω_s, Ω_k and Ω_ρ are the solid angles corresponding to the scattered and ejected electron momenta, and to the internuclear axis of the molecule, respectively. The N_e factor is the number of electrons in the considered MO. In view of exchange between electrons not being taken into account in the models, $N_e = 2$ for the reaction given in equation (33). As the target is considered frozen during the reaction effective time, the T-matrix transition element is computed at the internuclear equilibrium distance denoted by $\boldsymbol{\rho} = \boldsymbol{\rho}_0$. In the particular case of coplanar geometry, in which the ejected electron momentum is contained in the collision plane defined by the incident and scattered electron momenta, the FDCS reduce to five-fold differential cross sections (5DCS). Equation (35) is related to equation (3) for ion impact as for electron impact one has $\mu_i \cong 1$. Moreover, we are considering only reactions in which the conservation of energy is fulfilled, i.e. $E = E_i = E_f$, where E_i (E_f) is the initial (final) energy of the complete system as in the case of ion impact. In what follows, we consider the polar angles both for the ejected and scattered electrons to be taken as positive in the clockwise direction.

The initial non-perturbed wavefunction ψ_i is chosen according to,

$$\psi_i = \frac{e^{i\mathbf{K}_i\cdot\mathbf{R}_i}}{(2\pi)^{3/2}}\, \Phi_i \tag{36}$$

where $\mathbf{R}_i$ denotes the vector position of the incident electron with respect to the centre of mass of the molecule. Moreover, the plane wave with definite momentum $\mathbf{K}_i$ represents the fast incident electron and Φ_i is the two-electron initial molecular bound state described, for instance, by a simple Heitler–London type wavefunction [78]:

$$\Phi_i(\mathbf{x}_a, \mathbf{x}_b; \rho_0) = N_{HL}(\rho_0)\ \{e^{-\beta x_{a1}}\, e^{-\beta x_{b2}} + e^{-\beta x_{b1}}\, e^{-\beta x_{a2}}\}, \tag{37}$$

where we have labelled with $j = 1, 2$ and $j' = a, b$ the molecular centres and the molecule bound electrons, respectively. We denote by $\mathbf{x}_{j'}$ and by $\mathbf{x}_{j'j}$ the bound electron positions with respect to the centre of mass of the molecule and to the centre labelled by j, respectively. Moreover, $\rho_0 = 1.406$ au is the equilibrium distance of the H_2 ground state, $\beta = 1.166$ and N_{HL} is the normalization constant (depending parametrically on ρ_0).

Consequently, the perturbation in the entrance channel V_i is given by,

$$V_i = \frac{1}{s_a} + \frac{1}{s_b} - \frac{Z_T}{R_1} - \frac{Z_T}{R_2}, \tag{38}$$

where $\mathbf{R}_j$ and $\mathbf{s}_{j'}$ are the position vectors of the incident electron with respect to the centre labelled j and with respect to the bound electrons labelled j', respectively. In equation (38), $Z_T = 1$ is the charge of each molecular nucleus.

As in the case of heavy-ion impact, the first-order models we are presenting in this section were obtained by using a TEC approximation [79]. This approximation exploits the fact that, although bound electrons in the H_2 ground state are shared by the two nuclei, the electronic density is peaked around the nuclei positions. Then, it is assumed that the *active* electron is ionized from one centre while the *passive* electron (the one not ionized) is supposed to screen completely the nuclear charge of the other centre from which ionization is not produced. In this way, the exact final state Ψ_f^- is approximated by,

$$\Psi_f^- \cong \frac{\mathrm{e}^{\mathrm{i}\mathbf{K}_f\cdot\mathbf{R}_i}}{(2\pi)^{3/2}}\,\Phi_f\,\xi_c, \tag{39}$$

where the plane wave describes the fast scattered electron with momentum $\mathbf{K}_f$ and Φ_f stands for the final states of the residual H_2^+ molecular ion. In this section, we represent those states by a simple LCAO. For instance, the final *gerade* $^2\Sigma_g^+$ ground state of H_2^+ is described by,

$$\Phi_f = \Phi_g = N_g\ \{\phi_1 + \phi_2\} \tag{40}$$

where N_g is the normalization constant and ϕ_j represents a 1s-type hydrogenic wavefunction with variational charge Z^*= 1.3918 centred on either nucleus (labelled $j = 1$ or 2) of the molecule.

In the TEC model, the final continuum wavefunction ξ_c in equation (39) is taken as an effective Coulomb continuum function describing the motion of the ionized electron (from the center of mass of the molecule) in the Coulomb potential of the non-screened nucleus. Consequently, the final wavefunction in the TEC approximation reads,

$$\xi_c^{TEC}(\mathbf{k};\mathbf{x}_a,\mathbf{x}_{aj}) = \frac{\mathrm{e}^{\mathrm{i}\mathbf{k}\cdot\mathbf{x}_a}}{(2\pi)^{3/2}}\,C(\mathbf{k},\mathbf{x}_{aj},\gamma_e), \tag{41}$$

where we are supposing that the electron a is ionized from the j-centre without any loss of generality in the modelization employed [79]. The Coulomb factor denoted by $C(\mathbf{k},\mathbf{x},\gamma)$ is given by,

$$C(\mathbf{k},\mathbf{x},\gamma) = \Gamma(1-\mathrm{i}\gamma)\,\mathrm{e}^{-\pi\gamma/2}\,{}_1F_1[\mathrm{i}\gamma;1;-\mathrm{i}(kx+\mathbf{k}\cdot\mathbf{x})], \tag{42}$$

where we have defined the following Sommerfeld parameter:

$$\gamma_e = -Z_T/\mathrm{k}. \tag{43}$$

TEC results are in reasonable good agreement with measured cross sections [79] constituting thus a reliable description of the dynamics of the reaction given by equation (33). In order to take into account the Coulomb interactions between the pairs of charged fragments present in the final channel of the reaction, a more elaborated model was introduced, the so-called molecular BBK approximation (MBBK) [80]. In the MBBK model, the final continuum wavefunction includes a product of three Coulomb functions associated to the three two-body pairs present in the final channel, which we assume to have three bodies, i.e., the scattered and ejected electrons, and the residual target taken as a whole body. The MBBK final wavefunction was inspired by the atomic model (BBK) developed by Brauner, Briggs and Klar [81] for light particles and by Garibotti and Miraglia for heavy-ion impact [82]. The final wavefunction in the MBBK model is then given by

$$\xi_c^{MBBK}(\mathbf{k},\mathbf{K}_f;\{\mathbf{x}\}) = \frac{\mathrm{e}^{\mathrm{i}\mathbf{k}\cdot\mathbf{x}_a}}{(2\pi)^{3/2}}\,C(\mathbf{k},\mathbf{x}_{aj},\gamma_e) \times C(\mathbf{K}_f,\mathbf{R}_j,\gamma_f)C(\mathbf{k}_a,\mathbf{s}_a,\gamma_a) \tag{44}$$

where $j = 1$ or 2 indicates the centre from which the target electron is assumed to be ionized and $\{\mathbf{x}\}$ denotes the ensemble of coordinates used in the description of the final state. Moreover, the following Sommerfeld parameters are defined,

$$\gamma_f = -Z_T/K_f \qquad \gamma_a = \frac{1}{2k_a}, \tag{45}$$

with $\mathbf{k}_a = \frac{1}{2}(\mathbf{K}_f - \mathbf{k})$, the momentum conjugate to $\mathbf{s}_a$, which denotes the position of the incident electron with respect to the electron labelled a.

It can be shown that the TEC and MBBK 5DCS, for a coplanar geometry for vertical transitions from the ground state of the initial ground state of H_2 to the final *gerade* ground state of H_2^+, reduce for sufficiently high enough impact energy to the following approximate expression [83, 84],

$$\sigma_g^{(5)} \simeq 2\,\left[1+\cos(\boldsymbol{\chi}\cdot\boldsymbol{\rho}_0)\right]\,\sigma_0^{(3)}, \tag{46}$$

where we define $\boldsymbol{\chi} = \mathbf{k} - \mathbf{q}$ and $\mathbf{q} = \mathbf{K}_i - \mathbf{K}_f$ being the momentum transfer. In equation (46) $\sigma_0^{(3)}$ represents a one-center triply differential cross section corresponding to *effective* atoms (with nuclear charge Z^*) placed at the position of either molecular nuclei [83]. Finally, we note that equation (46) is similar to equation (15), obtained for the case of heavy-ion impact.

3.2. Interference in triply and doubly differential cross sections

Coherent electron emission effects in the FDCS for electron impact were predicted by means of equation (46) for transitions from the ground state of molecular hydrogen H_2 to the final ground state of the H_2^+ residual ion [83]. As a matter of fact, interferences appear explicitly in the 5DCS given by equation (46) as a factor modulating the effective atomic cross sections denoted by $\sigma_0^{(3)}$. Some analogies with the characteristics pattern of Young's two-slit experiment and the one produced by this factor in which the two atomic H centres behave as a two-slit system separated by ρ_0 (the equilibrium internuclear distance of H_2) may be established. These analogies may provide a heuristic way in the search for interferences but any conclusion extracted from them must be handled with care keeping in mind that the presence of

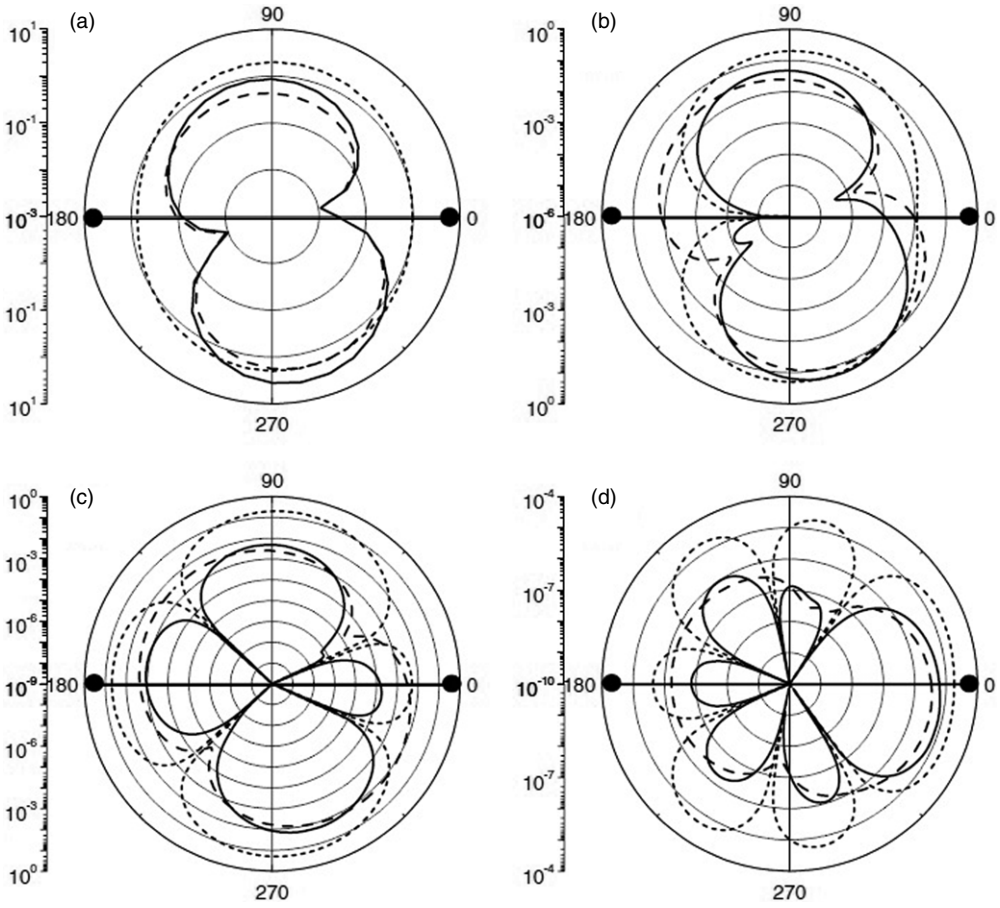

Figure 14. 5DCS as a function of the ejection angle, θ_e, for H_2 molecules aligned parallel to the incident beam. Impact energy, $E_i = 4087$ eV; scattering angle, $\theta_s = 1^\circ$; ejection energy, (a) $E_k = 20$ eV; (b) $E_k = 57$ eV; (c) $E_k = 100$ eV, and (d) $E_k = 500$ eV. Full curve: MBBK results. Dashed curve: two-effective H atoms. Dotted curve: interference factor (from equation (49)).

the momentum transfer q in the interference factor may play a crucial role as was previously discussed for heavy ions. In this way, interference effects are expected to manifest for de Broglie's wavelengths of the ejected electron similar to ρ_0. However, experimental verification of these effects is a formidable task as 5DCS given by equation (46) correspond to fixed-in-space molecules. Only recently experiments for oriented H_2 molecules were performed with the advent of reaction microscopes that allow to perform complete kinematic experiments in which the momenta of all fragments of the final reaction may be determined (we will discuss this point at the end of this section) [85]. Therefore, in order to compare with most of the experimental measurements for randomly oriented molecules, an average over all molecular orientations in the 5DCS is required. This procedure leads to averaged triply differential cross sections (3DCS) for a coplanar geometry which are given by,

$$\sigma_g^{(3)} = \frac{\mathrm{d}^3\sigma_g}{\mathrm{d}\Omega_k\,\mathrm{d}\Omega_s\,\mathrm{d}(k^2/2)} \cong 2\left[1 + \frac{\sin(\chi\rho_0)}{\chi\rho_0}\right]\sigma_0^{(3)}. \quad (47)$$

Integrating once more on all projectile scattering angles, DDCS are obtained,

$$\sigma_g^{(2)} = \frac{\mathrm{d}^2\sigma_g}{\mathrm{d}\Omega_k\,\mathrm{d}(k^2/2)} \cong 2\int \mathrm{d}\Omega_s\left[1 + \frac{\sin(\chi\rho_0)}{\chi\rho_0}\right]\sigma_0^{(3)}. \quad (48)$$

Equations (47) and (48) are related to equations (16) and (17) retrieved for the case of heavy-ion impact.

In the averaged 3DCS given by equation (47), the trace of interferences is encoded in the oscillatory factor,

$$\left[1 + \frac{\sin(\chi\rho_0)}{\chi\rho_0}\right] \quad (49)$$

which multiplies the effective one-center 3DCS given by $\sigma_0^{(3)}$.

In figure 14 we show 5DCS calculated using the MBBK approach for H_2 molecules with parallel alignment with respect to the incidence direction for electron impact energy E_i= 4087 eV, scattering angle $\theta_s = 1^\circ$ and ejection energies E_k= 20, 57, 100 and 500 eV. We also include in the panels results corresponding to two-effective H atoms given by $2\sigma_0^{(3)}$ and results corresponding to the interference factor given by equation (49). At the lowest ejection energy, i.e., E_k= 20 eV, the MBBK results are similar in a qualitative way to the ones of two-effective H atoms.

As the energy increases, that is to say, at shorter de Broglie's wavelengths for the ejected electron closer or lesser than the internuclear distance, new features are present that may be attributed to interferences. In particular, at $E_k = 57$ eV the MBBK 3DCS exhibit a zero for ejection at $\theta_e = 180^\circ$. It can be clearly seen in figure 14(b) that the origin of this node in the MBBK 3DCS comes directly from the interference factor

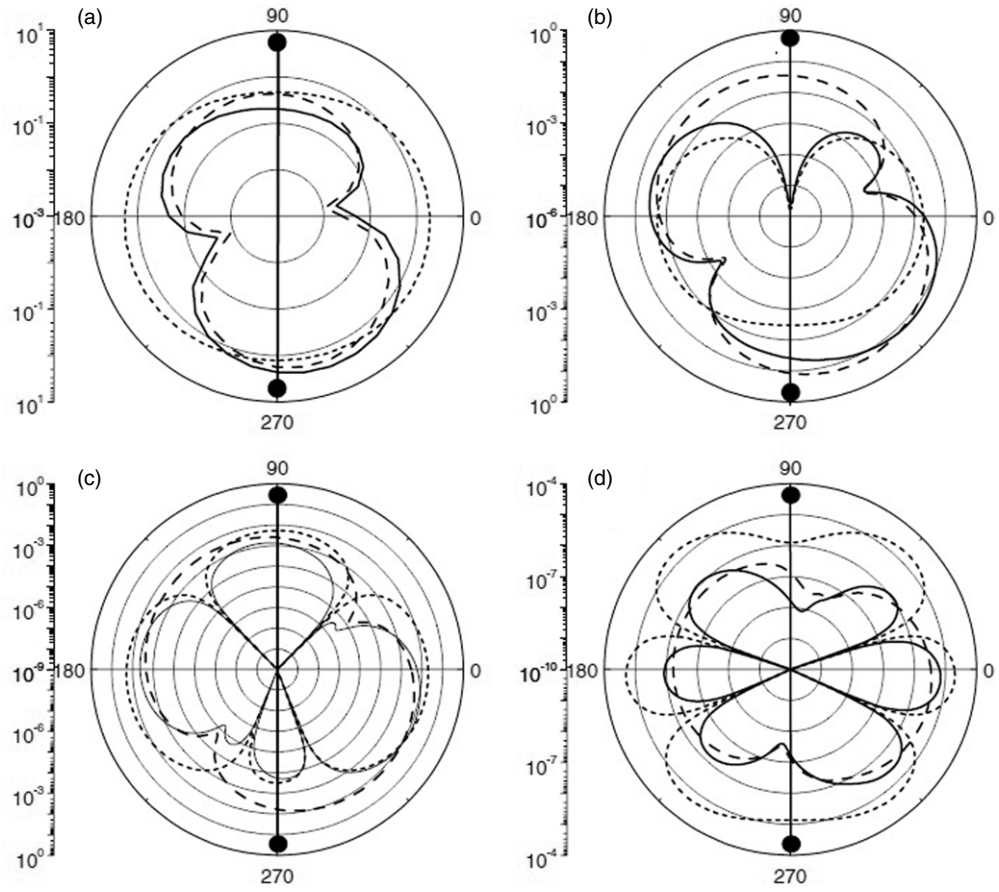

Figure 15. The same as figure 14, but considering the molecule oriented perpendicular to the beam direction. The ejection energy is (a) $E_k = 20$ eV, (b) $E_k = 51.2$ eV, (c) $E_k = 100$ eV, and (d) $E_k = 500$ eV.

in equation (49) changing in a dramatic way the behaviour of the two-effective atomic spectra. For greater ejection energies, the number of nodes increases. At $E_k = 100$ eV four nodes are predicted, at ejection angles $\theta_e = 21^\circ$, 136°, 224° and 339°, whereas at $E_k = 500$ eV six nodes are produced at $\theta_e = 56^\circ$, 100°, 156°, 204°, 260° and 304°. A similar situation occurs for molecules oriented perpendicularly with respect to the incidence direction as can be seen in figure 15. In particular, at ejection energy $E_k = 51.2$ eV a clear node is observed at ejection angle $\theta_e = 90^\circ$ in figure 15(b). As the energy increases, the number of nodes increases once again.

Therefore, it could be expected that these oscillations in the 5DCS manifest themselves through this factor also in the integration performed to obtain the DDCS given by equation (48). However, they still may be difficult to detect as the one-center cross sections decrease quickly with the impact energy and may hide them. In order to expose the oscillatory behaviour, the molecular cross sections may be divided by twice the corresponding effective one-center ones as it has been done in the case of heavy-ion impact.

The first experimental evidence for these oscillations for electron impact was obtained in the above mentioned way for collisions of 2.4 keV electrons impacting on deuterium molecules D_2 [86]. The experiments were carried out at CIRIL in Caen, France, using an electron gun of simple design in which the electron beam was directed into an effusive D_2 gas jet and collected in a Faraday cup, after passing through an exit slit [86]. To perform the experiment, the electron-spectroscopy apparatus from the Hahn–Meitner Institut in Berlin [87] was used, detecting the emitted electrons in the energy range from 2 to 2000 eV, at observation angles between 30° and 130°.

In figure 16, we show the experimental ratio between molecular DDCS for final D_2^+ ground state and twice the atomic ones as a function of the ionized electron at several emission angles together with theoretical results obtained with equation (48). A fit to experiments by employing a zero-order Bessel function is also included. There exist a general good agreement between the theory and experiment. It is worthy to note that maximum values of the 3DCS ratios (constructive interference) are expected for $\chi = 0$ (see equation (47)). This condition is satisfied in both soft collisions (corresponding to small momentum transfer, i.e., $k = q \cong 0$) and in the Bethe region (where all momentum is transferred to the ejected electrons, i.e., $k = q$). Then, these maxima values may give important contribution to the integration performed in equation (48) to obtain the DDCS. If interference effects were not present, the cross sections ratios at high incident energies would be approximately equal to unity. However, oscillations around unity in the DDCS ratios at emission angles $\theta_e = 30^\circ$, 110° and 130° are observed as the ejected electron velocity increases, putting in evidence the traces of interferences produced by the coherent electron emission from the two molecular centers. At the particular emission angle $\theta_e = 70^\circ$, experimental results at velocities greater

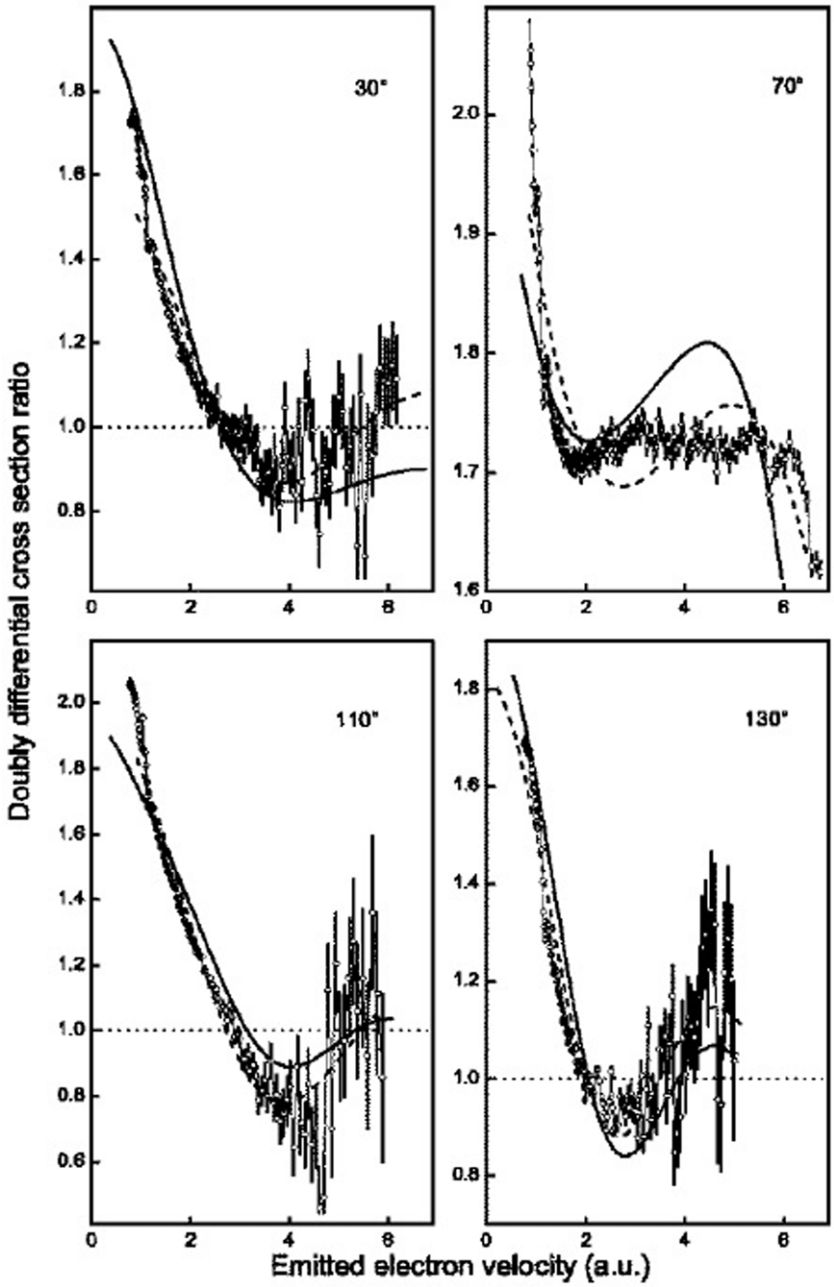

Figure 16. Experimental (open circles) and theoretical (full curves) doubly differential cross-section ratios for electron emission in 2.4 keV $e^- + D_2$ collisions as a function of the emitted electron velocity, for detection angles of 30°, 70°, 110°, and 130° [86]. Experimental ratios are fitted by using a zero-order Bessel function (dashed lines).

than 2 au give place to the formation of a *plateau* structure where the DDCS ratio oscillates around the 1.7 value. This particular behaviour comes from constructive interference effects around the binary peak region located at k=4.5 au, partially overlapping the constructive peak appearing at small k values.

After the completion of the first experiment exhibiting interference effects coming from the coherent superposition of electron emission from each molecular centre [86], the pursuit of new scenarios offering the possibility of detecting this type of quantum interference became an active field of research. In this way, experimental studies were conducted at Manchester University (UK) to ascertain whether 3DCS for single ionization of H_2 exhibit this kind of phenomena. Cross sections were then measured mainly for coplanar symmetric arrangements but also for a non-coplanar asymmetric collisions at low-intermediate impact energy (100 eV) [88]. These studies were not able to asses if interferences were responsible of the 3DCS features observed at the energy domain analysed. It must be noted that in those experiments the ejection energy employed was 5 eV, which corresponds to a de Broglie's wavelength for the ejected electron of approximately 10.4 au, that is much bigger than the internuclear distance $\rho = 1.4$ au, and there is thus little chance to observe interference effects. On the contrary, it was shown on the theoretical front and within the framework of

the distorted wave impulse approximation, supplemented with an averaged approximation for the MOs, that the Young-type double-slit interferences were indeed present (especially in the backward scattering region) for low-intermediate incident energy (75.6 eV) electrons impacting on N_2 molecules in non-coplanar asymmetric geometries [89]. In this work, the ejected and scattered electrons are considered to have the same energy (30 eV) and the asymmetric character of the reaction is determined by the asymmetry of their respective ejection and scattered angles. Let us remark that the equilibrium distance of N_2 molecules is about 2.1 au, that is to say, of the order of the de Broglie's wavelength (about 4.2 au) of the ejected or scattered electrons, and hence interference is expected to take place in a distinct way for these collisions. However, it was predicted in [89] that even if it were possible to perform an experiment with oriented molecules, no interference pattern would be observed for the coplanar symmetric case. In contrast, interferences were predicted to have a great influence on the 3DCS for equal energy coplanar asymmetric scattering if the N_2 molecule is oriented either parallel or normal to the incident direction, being the effect more important in the former case. Therefore, it was claimed that these facts are in accordance with the predictions of interferences for asymmetric conditions as given by equation (46). Furthermore, no Young-type interference was observed for a molecule oriented perpendicular to the incident direction and normal to the scattering plane. As the parallel orientation of the molecules dominates, interference effects remain also in the averaged 3DCS. Interestingly, analogies with some findings observed in photoionization of H_2 [90], that will be discussed in the next section, were established. Additional experimental and theoretical work on N_2 molecules suggested also the existence of two-centre interference effects [91]. Measurements were accompanied by calculations employing a M3DW and using an averaged oriented molecular approximation [92–94].

Experimental research on H_2 at higher impact energies (250 eV electron incident impact energy) developed at Griffith University (Australia), reported 3DCS for asymmetric collisions attributing their structure to constructive or destructive interferences [95]. Moreover, the experimental results exhibited a good agreement with the theoretical calculations obtained with a M3DW approach [92–94] employing also an averaged oriented MO approximation.

It has been argued that a decrease in the recoil peak intensity with respect to the binary one is due to interferences [95]. This particular finding promoted other intensive research to reach a final and conclusive answer. As a matter of fact, more experimental work to elucidate this point was carried out at Orsay (France) giving place to relative 3DCS for the ionization of the helium atom and the hydrogen molecule in coplanar asymmetric geometry for scattered electron energy of 500 eV and ejected electron energies of 205, 74 and 37 eV [96]. It must be noted that the de Broglie's wavelength of the ejected electron corresponding to those ejection energies are in the [1.6, 3.8] au interval, i.e., close to the equilibrium internuclear distance for H_2 (1.4 au), for which interference effects are expected to happen in a more evident way. After a direct comparison between the He and H_2 targets, oscillation

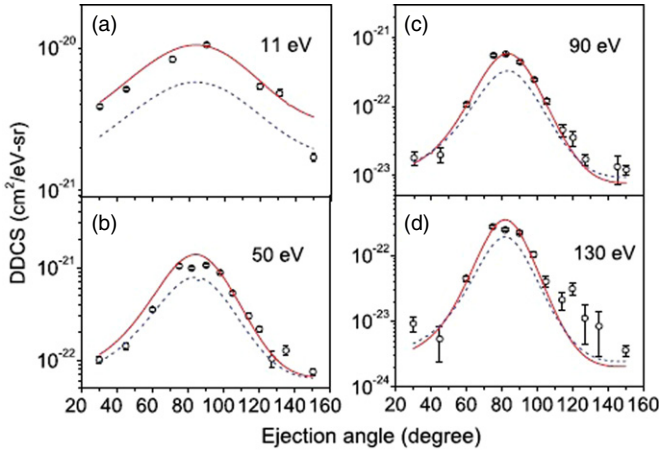

Figure 17. DDCS of electrons ejected at various angles between 30° and 150° for four different energies of (a) 11 eV, (b) 50 eV, (c) 90 eV and (d) 130 eV, respectively. The theory for molecular H_2 and twice the theoretical cross sections for two-effective H atoms are shown in solid and dashed lines, respectively. Statistical uncertainties are displayed in the experimental data [98].

patterns associated to the two-center nature of the target were identified. Moreover, constructive (for ejection energies of 205 eV) and destructive (for ejection energies of 37 and 74 eV) interferences depending on the wavelength of the ejected electron were measured [96]. In addition, experimental 3DCS were in good agreement with the predictions given by equation (47).

Later on, more evidence of constructive interferences were found at much higher impact energies at the soft and Bethe binary encounter regions [97, 98]. Experiments were performed at the Tata Institute of Fundamental Research (India), with an 8 keV electron beam impacting on H_2 targets where, for instance, absolute measurements of DDCS of ejected electrons with energies in the [1, 400] eV interval and ejection angles between 30° and 150° were reported [98]. The electron beam was prepared with a commercially available electron gun highly collimated by using several apertures and the emitted electrons were detected using an electron spectrometer equipped with a hemispherical electrostatic energy analyser and a channel electron multiplier. The energy resolution of the spectrometer was about 6% of the electron energy, limited by the entrance and exit apertures. More details on the experimental arrangement and spectrometer may be found in [97–99]. In figure 17, a general good accordance is observed between the TEC predictions and the absolute measured DDCS within the angular range of 30° to 150°. Deviations occur, however, at extreme forward and backward ejection angles as the ejection electron energy increases.

In contrast to highly charged heavy-ion collisions, the DDCS for electron impact exhibit a symmetric distribution with respect to the ejection angles that implies the absence of the post-collisional effects verified for the former ones [19, 106]. These post-collisional effects correspond to a preferable emission of the ionized electron in the direction of the projectile due to the strong attractive character of highly charged positive ions. It gives place to an increment of the yield in the forward direction compared to the backward

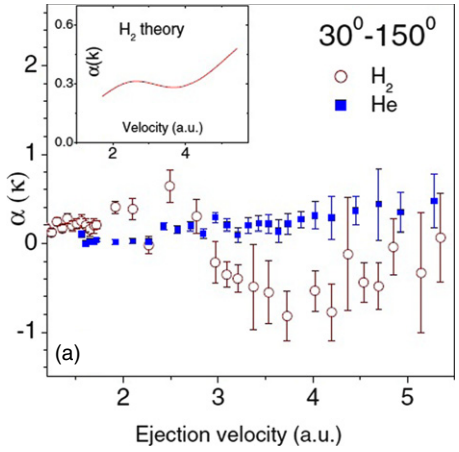

Figure 18. Asymmetry parameter given by equation (50) at $\theta_e = 30^\circ$ as a function of the ejection velocity for 8 keV electron impact on He (full squares) and H_2 (open circles) [97].

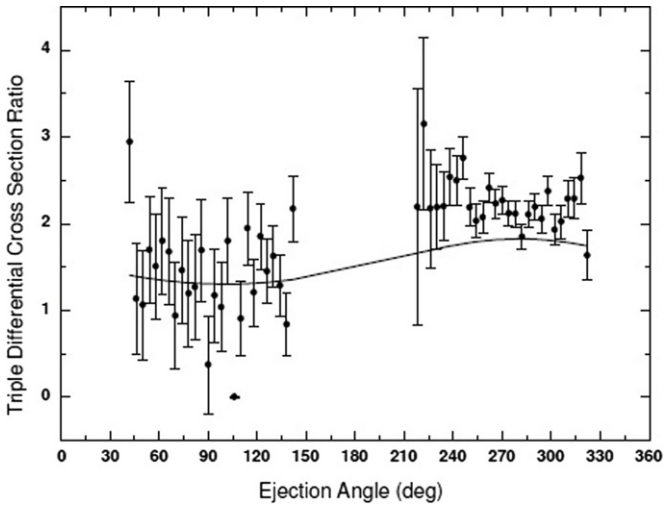

Figure 19. 3DCS ratios as a function of the ejection angle for $e^- + H_2$ at incident and ejection energies $E_i = 4087$ eV and $E_k = 20$ eV, respectively, and scattering angle $\theta_s = 1.5^\circ$. Full line, MBBK results [107]. Full circles, experiments obtained from [108].

angles. The clear differences between the effective atomic contribution and the molecular one at different angles may be ascribed to constructive and destructive interferences. In the soft-collision region (see the 11 eV case in figure 17) the theoretical atomic cross sections underestimate both theoretical and experimental molecular cross sections by about 30%–50% indicating constructive interference within experimental uncertainties. Similarly, in the Bethe binary-encounter regions around 90° the atomic cross sections underestimate the molecular one by 30%–40%, which suggests the existence of partial constructive interference. Although not shown here, the constructive interference dominates in the Bethe region even for larger ejection electron energies (see e.g figure 7 of [98]). Moreover, the search of constructive interference in the binary encounter peak was extended to the study of (H_2/He) ratio showing also undulations ranging from 0.5 to 2 that may be understood as the summed contributions of the Compton profiles and the interference effects [113]. These studies support the fact that the cross section at the binary peak for H_2 is enhanced by the constructive interference originated by the coherent electron emission from the two H centers of the molecule [113].

In addition, an asymmetry parameter analysis was performed as the one previously developed for heavy-ion impact [104]. In the latter case, it is known that the long-range Coulomb interactions between the residual target and the (highly) charged ion with the final state electrons create a two-center effect provoking a forward focusing in the electron emission. As a result, electrons are emitted preferentially in the forward direction. However, for electrons as projectiles the scenario is quite different [97]. As in equation (21) for heavy-ion impact, we define an asymmetry parameter α as,

$$\alpha(k) = \frac{[\sigma(k,\theta_e) - \sigma(k,\pi - \theta_e)]}{[\sigma(k,\theta_e) + \sigma(k,\pi - \theta_e)]} \qquad (50)$$

where now σ represents the DDCS given by equation (48). In figure 18, we show experiments for 8 keV electron impact on both H_2 and He targets [97]. In the inset, we present the theoretical prediction for H_2 in agreement with the experimental results concerning phase and frequency of the oscillation. The asymmetry parameter for He exhibits a smooth linear behaviour with the ejection velocity. On the contrary, the one for the molecular target presents clear undulations around a horizontal line around zero that may be related to the difference of frequencies of first-order oscillations of the two complementary angles involved in the measurements (30° and 150° in this case) as explained earlier in [104] for heavy-ion impact. In contrast, the oscillations for heavy-ions impact on H_2 are produced all along a straight line with a steep slope. This distinctive feature could be attributed to the post-collisional two-center effect [19, 105, 106]. In this way, for heavy-ion impact the asymmetry parameter for H_2 encodes at the same time as both the two-center post-collision and interference effects. For the one-center He target, no undulations are observed and only a monotonically increasing function is recorded with a slope similar to the one for H_2 [105]. This is in sharp contrast to the almost horizontal behaviour for electron impact as can be seen in figure 18. After what has been exposed, one may conclude that the oscillations in the asymmetry parameter for electron impact on H_2 are basically originated by interferences with negligible action of the post-collisional two-center effect. In this way, the electron-H_2 system reveals as a performer benchmark system to study exclusively coherent electron emission.

Oscillations in the 3DCS given by equation (47) were also analysed as a function of the ejection angle for definite scattering and emission energies [107]. In figures 19 and 20, collisions of 4.087 keV electrons impacting on hydrogen molecules were studied for ejection electron energy E_k = 20 eV and 3DCS for scattering angles $\theta_s = 1.5^\circ$ and 3° are presented, respectively. Good qualitative agreement is observed between theoretical predictions and experimental ratios obtained from the 3DCS of [108]. For $\theta_s = 1.5^\circ$, the theoretical 3DCS ratio oscillates around 1.5, exhibiting a maximum value of approximately 1.7 around the binary peak region. It is worthy to mention that with our angles convention, for $\theta_s = 1.5^\circ$ (3°), the binary peak region lies around 280°

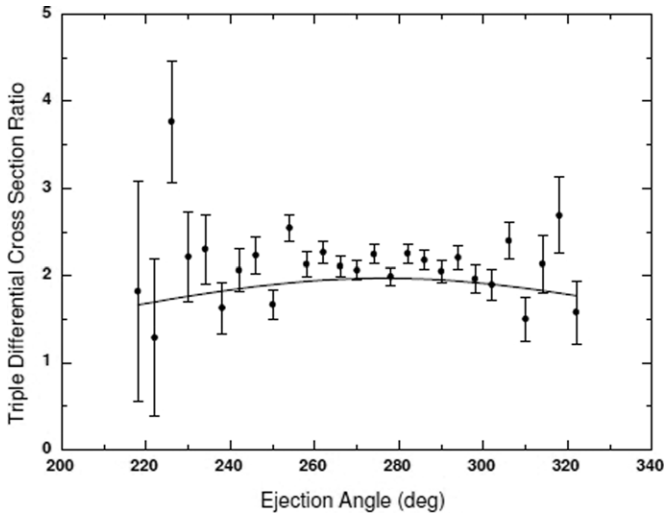

Figure 20. Same as figure 19 but scattering angle $\theta_s = 3^\circ$.

(277°). The available measurements tend to corroborate this tendency. At $\theta_s = 3^\circ$, theory presents a maximum close to 2 again around the binary peak region. Experimental results are distributed around this maximum value.

3.3. Interference in singly differential cross sections

Besides evidence of the interference effects in the DDCS, it was also shown that their trace remains even in singly differential cross sections (SDCS) [98]. For instance, after integrating the DDCS given by equation (48) over all ejection angles, SDCS as a function of the ejection energy may be obtained. Alternatively, SDCS as a function of the scattering angle may be also computed as,

$$\frac{\mathrm{d}\sigma}{\mathrm{d}\Omega_s} \cong 2 \iint \mathrm{d}\Omega_k \, \mathrm{d}(k^2/2) \left[1 + \frac{\sin(\chi\rho_0)}{\chi\rho_0}\right] \sigma_0^{(3)}. \qquad (51)$$

We present in figure 21, SDCS as a function of the scattering angle for electrons emitted in the 8 keV $e^- + H_2$ collision system. It can be seen (upper part) that the theoretical effective atomic cross sections lie below both the experimental and theoretical molecular cross sections. This constitutes an indication of the presence of partial constructive interference in the SDCS spectrum at almost all detection angles. The experimental SDCS ratio (H_2/2H) (shown in the bottom part of the figure) is close to the theoretical predictions which are almost constant around the 1.5 value. Although not shown here, remnants of the coherent electron emission have been also identified in SDCS as a function of the ejected electron energy resulting from integrating the DDCS over all scattering angles [98].

3.4. Suppression of the binary and recoil peaks by interferences

In the preceding sections, we have reported the main efforts to look for evidences for interference effects related to the two-center nature of various diatomic molecules. In general, they were traced back by means of distinctive oscillations in the cross sections (or, alternatively, in the asymmetry parameter).

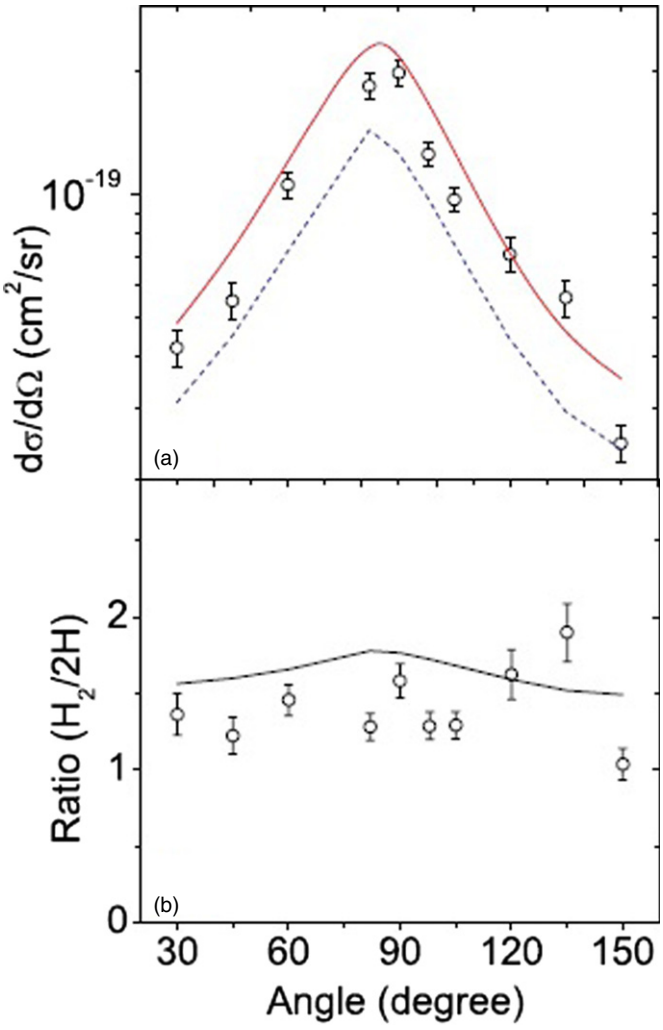

Figure 21. (a) SDCS as a function of the scattering angle in the 8 keV $e^- + H_2$ collisions. Theoretical molecular cross section, solid line. Twice the theoretical effective atomic cross section, dashed line. (b) Open circles: ratio of experimental SDCS and twice the theoretical SDCS for two-effective H atoms; solid line: theoretical SDCS ratio. All results from [98].

In this section, we report an astonishing consequence of interferences, i.e., the suppression of the so-called binary and recoil peaks, that can be considered as a unique signature of coherent electron emission from molecular centers.

As is well known, electronic emission by impact of massive particles is most probable in the direction given by the momentum transfer **q**. Classical ionization mechanisms manifest in the FDCS by the presence of a prominent peak, the so-called binary peak, and another one, usually lower than the binary one, recognized as the recoil peak observed in almost the opposite direction at which the binary peak appears. The latter may be associated to a classical binary collision between the projectile and the active electron whereas the recoil one may be related to a two-step mechanism in which the active electron suffers a binary collision with the projectile and then the electron is backscattered elastically by the target nucleus which in turn recoils to conserve the total momentum. It was an accepted assertion that the binary and recoil peaks must appear in every FDCS at sufficiently

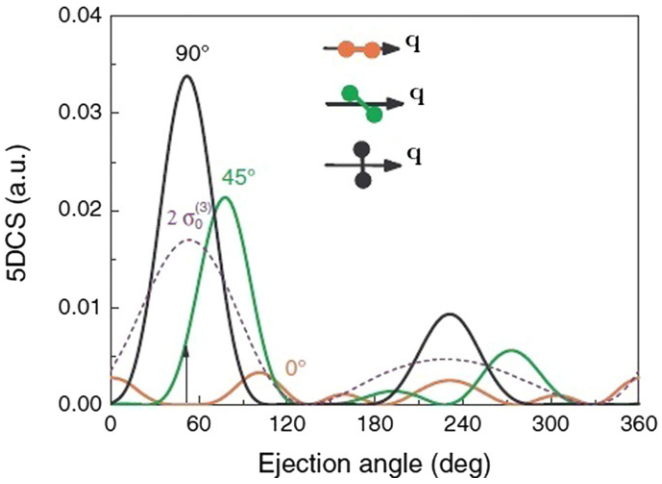

Figure 22. 5DCS as a function of the ejection angle θ_e for initial H_2 ground state oriented at 0° (red line), 45° (green line) and 90° (black line) with respect to the momentum transfer **q**, and for the final H_2^+ *gerade* state. Impact and ejection energy are $E_i = 4087$ eV and $E_k = 93.8$ eV, respectively, $\theta_s = -1°$ scattering angle. The positive orientation for the polar angles is taken clockwise. Full lines, MBBK results. Dashed lines, twice effective atomic cross sections [84]. The arrow over the *x*-axis indicates the classical binary peak position.

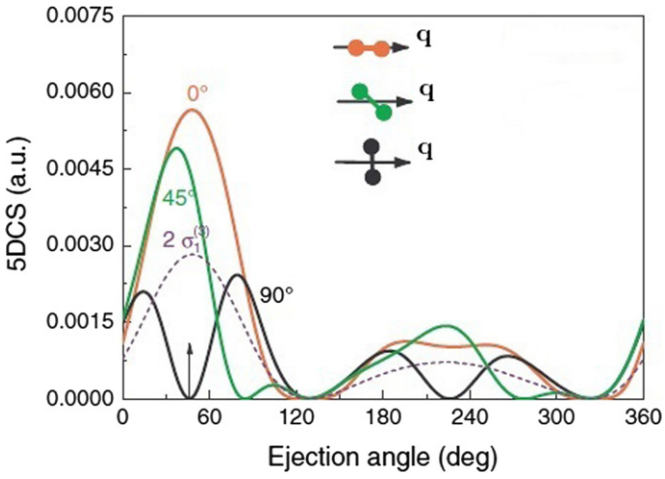

Figure 23. Same as figure 22 but for the final first excited *ungerade* state of H_2^+ [84].

high impact energy for atomic as well as for molecular hydrogen as an underlying fingerprint of classical mechanics in the quantum predictions [109]. It must be mentioned that only under particular conditions, the so-called Bethe ridge conditions, all the momentum is transferred to the ejected electron and no recoil peak is observed in accordance with classical mechanics. However, it is not possible to realize any classical mechanism that can lead to the absence of the binary peak for atomic nor molecular targets. As a matter of fact, ionization of ground state atomic hydrogen by electron impact [81] exhibits clearly the aforementioned peaks both in the experimental and theoretical results. The same happens for ground state molecular hydrogen targets leading to ground state H_2^+ residual targets in the final channel (see for instance [79, 80]).

Nevertheless, in what follows we will report the unexpected fact that the binary or recoil peak may be suppressed in ionization of molecular hydrogen erasing the traces of the classical mechanics in the observables of the reaction by virtue of destructive interferences. In figure 22, we present the MBBK results for ionization of H_2 ground state molecules [84] as a function of the ejection angle θ_e for vertical transitions to the *gerade* ground state of the residual H_2^+ molecular ion. Results are obtained in an approximated way by neglecting the so-called indirect terms [80]. The impact and emission electron energies are $E_i = 4087$ eV and $E_k = 93.8$ eV, respectively, whereas the scattering angle is fixed at angle $\theta_s = -1°$. It is worthy to mention that with our angles convention, for $\theta_s = -1°$ the binary peak region lies around 51.4°. We consider three orientations of the molecule with respect to the momentum transfer direction, namely 0°, 45° and 90°. Typical interference patterns caused by the coherent electron emission from the two molecular centres are observed as pointed out previously [83] when compared with effective atomic cross sections $\sigma_0^{(3)}$. As expected, the binary and recoil peaks can be seen for molecules oriented at 45° (green line) and 90° (black line). What is surprising now is that *the binary peak is practically suppressed for molecules oriented in the* **q** *direction*. Therefore, ionization in the classical predicted direction is forbidden. This shocking effect is produced by destructive interferences originated by the coherent scattering from both molecular centres. Indeed, the interference factor in equation (46) predicts total destructive interference when the condition $\boldsymbol{\chi} \cdot \boldsymbol{\rho}_0 = l\pi$ is verified for odd l values satisfying conservation laws. For the kinematical conditions analysed in figure 22, it can be shown easily that $k \sim l\pi/\rho_0 + q$ for molecules aligned in the momentum transfer direction. This result can be related to the one obtained for photoionization of H_2 [100], where it was shown that no photoelectrons are emitted if a similar relation holds for molecules aligned along the polarization direction of the incident radiation, i.e., the classically expected direction for photoelectron emission.

Let us consider now the case of the first excited *ungerade* final state of the H_2^+ residual target for which the 5DCS is similar to the one given by equation (46) [84, 101],

$$\sigma_u^{(5)} \simeq 2[1 - \cos(\boldsymbol{\chi}.\boldsymbol{\rho}_0)]\, \sigma_1^{(3)}, \tag{52}$$

where $\sigma_1^{(3)}$ represents a one-center triply differential cross section corresponding to effective atoms (with nuclear charge Z_1^*) placed at the position of either molecule nuclei [84].

We present in figure 23 MBBK results for transitions to the the first excited $^2\Sigma_u^-$ final (*ungerade*) state of the residual H_2^+ target [84] for the same kinematical conditions as in figure 22. The most important feature is that *the binary and recoil peaks are suppressed for molecules with their axis normal to the momentum transfer*. From equation (52), the condition for this suppression is given by $\boldsymbol{\chi} \cdot \boldsymbol{\rho}_0 = \pm n\pi$ for n an even number. In particular, this condition is valid for $n = 0$ leading to the conclusion that regardless of the impact and ejected energies, electrons cannot be ejected perpendicularly to the internuclear axis for molecules oriented normal to the **q** direction for this *ungerade* state. Therefore, a nodal plane for electron ejection just in the classical direction of emission is observed for final

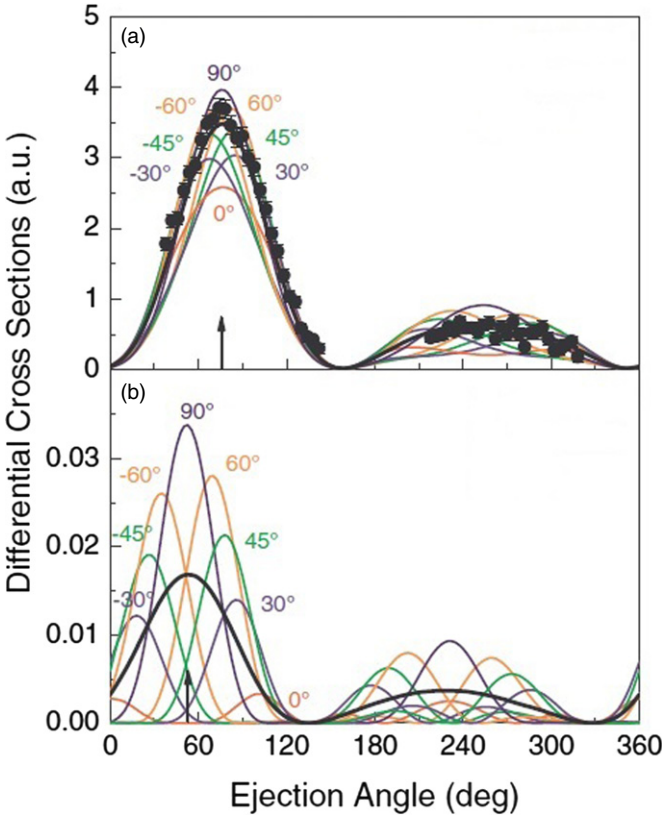

Figure 24. 5DCS as a function of the ejection angle θ_e for initial H_2 ground state and final H_2^+ ground state averaged over all molecular orientations for a coplanar geometry at incident and ejection energies $E_i = 4087$ eV and $E_k = 20$ eV, respectively, and scattering angle $\theta_s = -1^\circ$ (positive orientation for the polar angles is taken clockwise). MBBK results, full line [84]. Experiments taken from [108]. Moreover, 5DCS for several molecular orientations with respect to **q** are included. (b) Same as panel (a) but $E_k = 93.8$ eV [84]. The arrows over the *x*-axis in both panels indicate the classical binary peak positions.

ungerade states. Finally, it was suggested that the emitted electron spectra from ground state H_2 molecules to final *gerade* or *ungerade* final state of the H_2^+ residual target are analogous to the interference spectra of two sources emitting coherently in phase or in opposition of phase, respectively [84].

Now, we are in position to pose a thought provoking question. Why the experimental 5DCS averaged over all orientations exhibit a peak just in the **q** direction whereas in figure 22 we see clearly a shift from the classical position for the maximum for molecules oriented at 45°? The answer may be derived from figure 24 [84] where we present MBBK 5DCS for several molecular orientations with respect to the momentum transfer. For orientation angles symmetric with respect to **q**, the MBBK 5DCS are also almost symmetric. As all orientations are equally probable, the average obtained by integration over them gives place to a maximum around the position of the classically predicted binary peak measured in experiments. This can be seen clearly in figure 24(a) where we exhibit the way the contributions at different angles *build* the binary peak. The same situation is observed in figure 24(b) where the de Broglie's wavelength of the ejected electron is shorter and more pronounced interference effects are expected, leading even to the suppression of the binary peak as we have already discussed. However, the average over all molecular orientations gives again a peak at the classical position.

Even if the claims of this subsection have been inferred with first-order models for ionization employing simple descriptions for the molecular states, there is every reason to believe that the main physics underlaying the dynamics of the reaction has been properly considered. Unfortunately, there do not exist, till now, experiments to confirm our theoretical findings. However, in the age of reaction microscopes [16, 110] it is not difficult to envisage in the near future experiments with oriented molecules (involving final dissociative states such as the ungerade state here studied) to corroborate them. As a matter of fact, recently multiple differential cross sections for ionization of aligned hydrogen molecules in ground state by electron impact were accomplished [85, 111, 112]. By means of a reaction microscope, the complete kinematics of the reaction is determined and, at the same time, the molecular orientation is obtained from dissociation of the residual ion. In particular, multiple differential cross sections as a function of the polar angle of emitted electrons were measured at lower incident energy of 200 eV and ejection energy of (3.5 ± 2.5) eV for molecules aligned in the scattering plane at angles of 0°, 45° and 90° with respect to the momentum transfer [85] and scattering angles of $(5 \pm 2)^\circ$, $(9.5 \pm 2.59)^\circ$ and $(16 \pm 4)^\circ$. Due to limitations in the experimental design, data only around the binary (30° to 130°) and recoil regions (230° to 330°) were recorded. Moreover, M3DW calculations in which a Dyson orbital formalism is used to describe the MOs together with an initial-state spherically symmetric distorting potential to determine the initial-state distorted wave [85, 111], were presented. To perform the calculations, it was taken into account that the ground state dissociation of the residual ion produced during the reaction is almost identical to non-dissociative single ionization of H_2 but occurring at sub-equilibrium internuclear distances of about 1.1 au [85, 111]. Then, in the computation of cross sections, the final state is taken as the one corresponding to the ground state of H_2^+ but considering the mentioned sub-equilibrium internuclear distance. As the experimental results were not on an absolute scale, the M3DW ones were used to normalize them before the comparison between experiment and theory was performed. On one hand, discrepancies appear in the contrast experiment-M3DW theory, although there exists a qualitative agreement for the three molecular alignments analysed. On the other hand, it has been pointed out that the equation (46) gives multiple differential cross sections with similar values to the experimental and M3DW results but differing on the ordering at the binary and recoil peaks for the three studied molecular orientations. However, it must be kept in mind that equation (46) is valid at sufficiently high impact energies where the indirect terms may be neglected [80]. At the impact energies involved in the aforementioned experiments, the application of the TEC and MBBK models may not be justified. Surprisingly, these models reproduce the ordering observed in experiments for final dissociative ungerade states as shown in figure 23 [84, 101]. Nevertheless, a proper comparison with experiments requires inclusion of

the neglected indirect terms and also a correct description of the final dissociative state.

In recent contributions, Young's double-slit type interferences for quantum particles was revisited. In the work by Baltenkov *et al* [102], it is claimed that the analogy with the double-slit experiment was exaggerated as emission of electrons from diatomic molecules exhibits particular features which are not present in the two-slit interference patterns. This conclusion is reached after comparing the results of the classical interference of an electron scattered by two spatially separated centers with molecular photoelectron angular distributions. As a matter of fact, specific characteristics for the impact of heavy-ions and electrons have been also pointed out in the preceding paragraphs and other ones will appear in the next sections. Nevertheless, the image of the two-slits experiment may be helpful at least at sufficiently high impact energies to get a better understanding of the mechanisms involved in the coherent electron emission processes.

Finally, Ozer *et al* [103] performed calculations within the M3DW approximation to analyse interferences in the ionization of hydrogen molecules by impact of 250 eV electrons. Results for both an energy range with a fixed projectile angle and a projectile angle range with a fixed ejected electron energy are presented. In addition, experiments performed at the Afyon Kocatepe University, Turkey, for molecular hydrogen and also for He atoms (used to obtain experimental cross section ratios) were reported. They found that the interference factor has a richer structure than the one predicted by the simple Cohen and Fano model (see next section). This fact may be also understood as the impact energy analysed in that work could be not high enough to ensure the use of equation (47). In the same line of findings anticipated by Alexander *et al* for proton impact [58], they conclude that interferences exhibit a stronger dependence on the projectile scattering angle than on the ejected electron energy.

4. Photons as projectiles

As mentioned in the introduction, interference effects coming from the coherent emission from diatomic molecules were first suggested by Cohen and Fano (CF) [15] as early as 1966, in order to explain oscillations obtained in experimental photoabsorption spectra of nitrogen (N_2) and oxygen (O_2) molecules [121]. They assumed that ionization is basically a one-electron process focusing their attention on the particular case of H_2^+ molecules and developing a first-order model in which the ejected electron is described as a free one-center spherical wave and the molecular states are represented by a simple LCAO. After the first experiment providing evidence of these kind of interferences for heavy-ion impact in 2001 [12] and with the knowledge gained through the research of coherent emission induced by heavy-ions and electrons as exposed in the preceding sections, photoionization was revisited in several works in order to go deeper in the understanding of these interference phenomena [39, 100, 114, 115]. One would expect notable coherent electron emission effects with diatomic molecules when the de Broglie's wavelength of the photoelectron is similar to their internuclear distances. As the latter are within the order of 1 au, this is equivalent to having incident photon energies of hundreds of eV currently available in radiation synchrotron and free electron lasers facilities. In contrast with massive projectile impact, ionization by photon impact does not lead a scattered particle in the final channel of the reaction as the initial photon is absorbed and its energy is shared between the ejected electron and the degrees of freedom of the residual molecular target with no momentum transferred within the dipole approximation. In addition, symmetry requirements reduce greatly the population of the final states. As a matter of fact, if ionization of $^1\Sigma_g^+$ ground state hydrogen molecules is considered, then only final continuum $^1\Sigma_u^+$ and $^1\Pi_u$ states are allowed due to the dipole selection rule.

4.1. Interferences in multiple differential and total cross sections

The dipole matrix transition element from which PCS may be calculated is given by,

$$T_{\alpha lm\mu}(\varepsilon) = \int \mathrm{d}\rho \langle \Psi_{gv}(\mathbf{x}, \rho) | \mathbf{e}_\mu \cdot \mathbf{D} | \Psi^+_{\alpha \upsilon_\alpha lm\varepsilon}(\mathbf{x}, \rho) \rangle, \quad (53)$$

where Ψ_{gv} denotes the ground molecular state of energy W_{gv} and $\Psi^+_{\alpha\upsilon_\alpha lm\varepsilon}$ represents the final molecular state of energy $W_{\upsilon_\alpha} + \varepsilon$ describing a molecular ion in the υ_α vibrational state and an emitted electron with energy and angular momentum ε and lm, respectively. Moreover, $\mathbf{x}$ denotes the electronic coordinates, ρ represents the internuclear distance, $\mathbf{e}_\mu$ is the polarization vector of the incident photon, and $\mathbf{D}$ is either $\sum_i \mathbf{x}_i$ (length gauge) or $(\hbar\omega)^{-1} \sum_i \nabla_i$ (velocity gauge). Furthermore, conservation of energy leads to $W_{gv} + \hbar\omega = W_{\upsilon_\alpha} + \varepsilon$. Disregarding rotational effects, the wavefunctions Ψ_{gv} and $\Psi^+_{\alpha\upsilon_\alpha lm\varepsilon}$ are computed within the adiabatic Born–Oppenheimer (BO) approximation:

$$\Psi_{n\upsilon_n}(\mathbf{x}, \rho) = R^{-1} \chi_{\upsilon_n}(\rho) \psi_n(\mathbf{x}, \rho), \quad (54)$$

with ψ_n and χ_{υ_n} denoting the usual electronic and nuclear BO wavefunctions, respectively [116, 117]. Multiple differential PCS as a function of the the energy and direction of the ejected electron, and the energy and orientation of the residual H_2^+ molecular ion were obtained through the Dill's formula [120] employing the transition dipole matrix element given by equation (53).

The wavefunctions appearing in the matrix element given by equation (53) are constructed by means of B-splines computational techniques [116, 117]. In particular, the vibrational (bound and dissociative) wavefunctions are developed in a basis consisting of 280 B-splines of eight order contained in a box of 12 au. A detailed description of the evaluation of the electronic wavefunctions may be found in [116, 117]. In a concise way, the ground state Ψ_g is obtained from a configuration interaction scheme in which the H_2 Hamiltonian has been diagonalized in a basis of 321 configurations built from products of one-electron H_2^+ orbitals and pseudo-orbitals. The resulting energy at the equilibrium internuclear distance is $-1.886\,5023$ au very close to the exact non-relativistic value $-1.888\,761\,38$ au [118]. All these orbitals are described by using a one-center development

including spherical harmonics up to $l = 16$. The associated radial functions have been expanded on a basis of 310 B-splines of eight order in a box of radial length of 60 au. The final electronic continuum state $\Psi^{+}_{\alpha\upsilon_\alpha lm\varepsilon}$ is obtained from a close-coupling calculation including partial waves with $l \leqslant 7$ associated to the four lowest ionization thresholds of H_2: $X^2\Sigma_g^+(1s\sigma_g)$, $^2\Sigma_u^+(2p\sigma_u)$, $^2\Pi_u(2p\pi_u)$ and $^2\Sigma_g^+(2s\sigma_g)$. For every value of ρ, these continuum states satisfy the usual boundary conditions corresponding to (i) one electron in a bound electronic state of H_2^+ and (ii) the remaining electron in a single outgoing spherical wave with a well defined value of the angular momentum l plus a combination of incoming spherical waves for all accessible electronic states of H_2^+ and all allowed values of the angular momentum of the ejected electron according to the molecular symmetry [116]. Therefore, the molecular states are represented by means of this *ab initio* procedure in a realistic way including electron correlation and the two-center character of the molecular potential in all bound and continuum wavefunctions. At first, a close-coupling calculation within the fixed nuclei approximation (i.e., neglecting the vibrational degrees of freedom of the molecule), including open channels associated to the lowest ionization thresholds of H_2, was employed to obtain the final continuum state [39] in order to validate the CF hypothesis and their findings. The convergence of the total PCS (TPCS) was tested by comparing 4-channels results with 10-channels ones, the latter ones giving almost the same results as the former ones. It was observed that $^1\Pi_u$ contributions present a monotonous decrease as a function of the photon energy whereas $^1\Sigma_u^+$ contributions exhibit a non-monotonous behaviour [39]. Moreover, it was shown that the different thresholds contributions to the $^1\Sigma_u^+$ PCS is dominated by the threshold $X^2\Sigma_g^+(1s\sigma_g)$. Therefore, this proves that the reaction is mainly a one electron process without excitation of the non-ionized electron in agreement with CF basic assumptions [15]. Moreover, theoretical H_2 to twice atomic hydrogen TPCS were analysed in the search of interference patterns. As can be seen in figure 25, oscillations are observed as the photon energy increases. In order to get a better comprehension of the physical origin of these oscillations, we have performed a fit to the 4- and 10-channels predictions by using the following CF-type ratio,

$$a_0[1 + \sin(ka_1)/(ka_1)] \tag{55}$$

with a_0 and a_1 taken as free parameters. The result of the fit ($a_0 = 1.46$ and $a_1 = 1.57$) is included in figure 25. The good agreement between the fit and the theoretical results at high photon energies supports the physics underlying in the CF model. However, its quantitative validity could be questioned as a_1 is slightly different from the equilibrium distance value ($\rho = 1.4$ au). Moreover, we remark that in the low-photon energy range the 4- and 10-channels results are in excellent agreement with the existing experimental data [121] representing the pronounced fall of the ratio as the photon energy decreases. As anticipated in the preceding sections, this fall in the measurements has been also reported for both ion and electron impact experiments. In contrast, the respective theoretical calculations are unable to explain it and

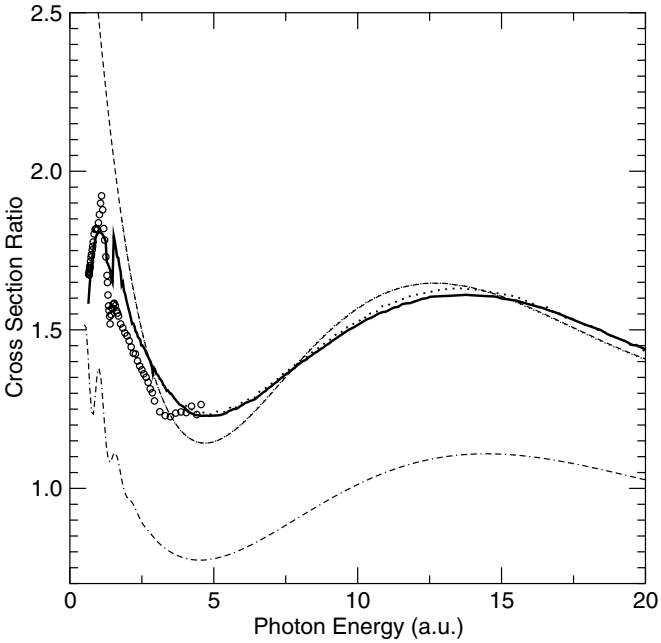

Figure 25. $\sigma_{H_2}/2\sigma_H$ photoionization ratio as a function of the photon energy [39]. Full line, 4-channel *ab initio* results. Dotted line, 10-channel *ab initio* results. Circles, experimental results by Samson and Haddad taken from [119] and divided by $2\sigma_H$. Dashed line, fit $\sigma_{H_2}/2\sigma_H$ to the Cohen-Fano formula. Dashed and dotted line, results for a fictitious one electron molecule with nuclear charges equal to 0.5; for the sake of clarity, the resulting curve has been multiplied by 0.25.

the same occurs for the CF-formula that increases as the photon energy diminishes. To elucidate the origin of this behaviour, we performed a B-spline calculation for a fictitious one-electron diatomic molecule with nuclear charges equal to $Z = 0.5$ and equilibrium distance $\rho = 1.4$ au, differing from the H_2 molecule only in the absence of correlation and/or screening [39]. These calculations describe adequately the TPCS ratio for high enough photon energies but do not reproduce at all the observed fall at lower ones. On the contrary, they present an overall increase of the TPCS as the photon energy diminishes. It was concluded that the origin of the fall in the TPCS ratio for low photon energies must be correlation and/or screening in the two-electron target states, regardless of the type of beam or mechanism that induces the electron ionization. It can be also concluded that a realistic description of the two-center nature of the molecular states is needed to properly describe the reaction verifying also the correct Coulomb boundary conditions. Briefly, it was shown for the first time that the CF model fails to describe TPCS for H_2 targets at least for low photon energies. Similar conclusions were obtained for H_2^+ targets but additionally it has been shown that the CF model is inadequate to describe the correct qualitative description of the interference effects observed at high photon energies [114]. It is worthy to mention that these results for both H_2^+ and H_2 molecules are only slightly changed if vibration of the nuclei is included in the computation of TPCS and the general conclusions remain the same [100, 115].

Subsequently, interference patterns were theoretically identified in a more direct way on the multiple differential

cross sections for the fixed-in-space molecules [100, 115]. Kaplan and Markin [122] were the first to draw the attention on this fact in 1969 and more recently Walter and Briggs [38] studied multiple differential cross sections by using a simple model in which the photoelectron is described by a plane wave and LCAO are employed to represent the molecular states neglecting the nuclear degrees of freedom. Although a difficult task, experiments with definite molecular orientations are now possible as explained in the previous section [85, 111, 127]. Nevertheless, theoretical work has shown that interference effects are clearly visible in the angular distribution of photoelectrons for molecules with a definite orientation in space. Even more, it has been proved that these effects depend critically on the final vibrational state of the residual target for linear polarization photons impacting on ground state H_2^+ and H_2 molecules [100, 115]. For molecules oriented normally to the polarization vector, the angular patterns can be related to the ones observed in the two-slit experiment whereas for molecules aligned in the polarization direction an interesting effect was predicted [100, 115]. The partial TPCS, i.e., cross sections corresponding to partial l waves of the photoelectron, exhibit a deep minima when the following relation is verified,

$$k\rho = l\pi \tag{56}$$

with k the photoelectron momentum and where the l quantized angular momentum is an odd number (in accordance with the dipole selection rules).

As the relation given by equation (56) corresponds to a particle confined in an infinite well of width ρ, this interference effect has been initially called *confinement effect*. After that, other works confirmed the existence of this effect for H_2^+ molecules considering it as a 'Cooper-like minima' for molecular targets [123, 124]. As is well-known, Cooper minima are basically observed in photoionization of atomic targets in $l \rightarrow l+1$ transitions due to the presence of at least one node in the initial radial atomic wavefunctions which causes the vanishing of the corresponding matrix transition element for definite conditions. However, it must be mentioned that the ground (gerade) molecular states involved in the reactions here analysed do not have any node. Consequently, these minima were called 'Cooper-like minima' in the case of molecular targets [123, 124] as they resemble the atomic case in the mathematical aspect, i.e., the matrix transition element is zero for definite conditions. The minima observed were also attributed to the non-spherical character of the molecular potential [114]. Many interpretations are possible but the important fact is that these minima are related to an interference effect coming from the two-center nature of the diatomic molecule [125]. In any case, we are facing an interference phenomena linked to the coherent electron emission from the two centres of the molecule and we could refer to it either as *confinement* or 'Cooper-like minima'.

More importantly, for the first time it was shown that the condition given by equation (56) has a critical implication if a final vibrational analysis is performed [100, 115]. Indeed, from the examination of the energy sharing between the residual target and the photoelectron, it is concluded that for particular final vibrational states photoelectron emission is forbidden in the polarization vector direction. For instance, for 2.5 au ($\simeq$ 68 eV) photons, practically no photoelectrons with $l = 1$, leaving the residual H_2^+ target in the fourth vibrational state, are emitted [100, 115]. This is surprising as the polarization direction is the classically expected direction for emission, i.e., the direction in which the electric field is acting on the electron. Therefore, this classical prediction is ruled out by quantum mechanical interference effects. Later on, a similar situation has been found for ionization of H_2 molecules by electron impact as we have anticipated in the preceding section.

4.2. Asymmetry parameters

Interference patterns were analysed also by defining averaged asymmetry parameters (β) that, varying between -1 and 2, measure the relative importance of the perpendicular and parallel components of the electric dipole transition, respectively. When the parameter value is $\beta = 2$, the angular distribution is mainly produced in the polarization direction whereas for $\beta = -1$ it is produced mainly perpendicularly to the polarization vector, β=0 being corresponding to an isotropic distribution [115, 126].

On one hand, it was found that an averaged electronic asymmetry parameter associated with the $^2\Sigma_g^+(1s\sigma_g)$ has practically a constant value $\beta \simeq 2$ for all photon energies, regardless of the inclusion or not of the dissociative channels. As the photon energy increases, some oscillations are produced but with such a small amplitude that their experimental detection would be very challenging [115]. On the other hand, the angular distribution of the H_2^+ ions produced in the photoionization of ground state H_2 targets was analysed by means of an averaged nuclear asymmetry parameter associated to the lowest ionization channel $^2\Sigma_g^+(1s\sigma_g)$ [115]. As the photon energy increases, this asymmetry parameter exhibits notable undulations that can be considered as an *echo* of the CF oscillations. This could be useful to characterize interference effects as proceeding in this way no atomic cross sections would be needed to define ratios. However, the obstacle to circumvent for such a procedure is the completion of an experiment with oriented H_2^+ molecular ions.

4.3. Vibrational analysis

Finally, the interference effects observed in the case of parallel alignment of H_2 molecules have an important consequence on the vibrational population of the H_2^+ residual target. At low photon energies (e.g., 20 eV), this vibrational distribution is expected to follow approximately a Franck–Condon (FC) distribution, which predicts that the $\upsilon = 2, 3$ vibrational levels should be the most populated ones. From the analysis of the vibrational distribution of the remaining H_2^+ ion on the dominant non-dissociative reaction, it is concluded that molecules oriented perpendicularly to the polarization vector follow closely an FC distribution [115]. In contrast, the molecules aligned with the polarization vector, exhibit clear deviations from the typical FC distribution. This violation of the FC prediction is closely related to the confinement effects above mentioned that produce an unexpected dominance of the

$l = 3$ partial wave over the $l = 1$ one for the lowest vibrational states [115].

Recently, Canton *et al* [128] showed that a direct observation of interferences coming from the coherent emission from the molecular centres may be accomplished in vibrationally resolved valence-shell photoionization of diatomic molecules. In particular, molecules such as H_2, N_2 and CO have been employed as targets and photoelectron spectra measured for photons with energies in the [21, 300] eV range by employing third-generation synchrotron radiation. It is shown that interferences originate oscillations in the corresponding vibrational ratios. In this way, the trace of the coherent electron emission is accessible in a direct way through the experimental results excluding possible ambiguities linked to the introduction of external parameters or fitting functions. The authors of this relevant work emphasize that this fact confirms the interpretation given by Cohen and Fano and they also asseverate that it is valid also for diatomic heteronuclear molecules.

5. Conclusions and outlook

We have reviewed in this contribution the state of the art of coherent electron emission from simple molecules by impact of energetic charged particles and photons. The electron emission can be initiated by heavy-ions, electrons or photons and we have analysed how an interference pattern emerges in different observable quantities. For each of these projectiles we have made a summary of several theories and explained all of them in detail. Furthermore, we have put emphasis both in the common factors and the differences. In general, the theoretical models are able to describe in some degree the experimental data and to give a clear interpretation of the interference phenomena. The latter have shown to be universal, in the sense that interference patterns seem to be present independently of the nature of the projectiles, once the adequate range of impact energies and final electron and projectile variables are chosen. Interestingly, we can consider the electron emission from the different molecular centers as the atomic counterpart of the double-slit experiment.

We can anticipate that the experiments using aligned molecules as targets will provide a stringent test for the theories and will open new theoretical and experimental avenues. In these systems, where a pump laser prepares the molecules in a highly aligned ensemble and the probe is now a fast charged particle or a photon, the interference effects will appear in a much cleaner way in the observables quantities. The experimental set up to perform this kind of experiments is still unavailable, but the constant growth in detection and laser techniques and the technological developments would make the measurements feasible in a not so far future.

Acknowledgments

MFC acknowledges the financial support of the MINCIN projects (FIS2008-00784 TOQATA and Consolider Ingenio 2010 QOIT). This work was partially supported by the National Science Foundation through a grant for the Institute for Theoretical Atomic, Molecular and Optical Physics at Harvard University and Smithsonian Astrophysical Observatory. OF and RDR acknowledge partial support from the Agencia Nacional de Promoción Científica y Tecnológica (Project PICT 2011 no 2145) and the Consejo Nacional de Investigaciones Científicas y Técnicas (PIP-CONICET no 1026/10), both institutions from the República Argentina. We fervently acknowledge J H McGuire, Y D Wang, S E Corchs, O L Weaver, J Hanssen, B Joulakian, R J Allan, A Motassim, H F Busnengo, M A Ourdane, N Stolterfoht, B Sulik, V Hoffmann, B Skogvall, J Y Chesnel, J Rangama, F Frémont, D Hennecart, A Cassimi, X Husson, A L Landers, J A Tanis, M E Galassi, P D Fainstein, G Laurent, L Adoui, A Cassimi, C R Stia, P F Weck, J Fernández, A Palacios, F Martín, O Kamalou, D Martina, C Dimopoulou, R Moshammer, D Fischer, C Höhr, J Ullrich, S Chatterjee, D Misra, A H Kelkar, L C Tribedi, J S Alexander, A C Laforge, A Hasan, Z S Machavariani, D H Madison, M Schulz, C A Tachino, S Kasthurirangan, A N Agnihotri, S Nandi and A Kumar for their collaborations with us on this topic, in some cases for more than twenty years.

References

[1] Young T 1807 *A Course of Lectures on Natural Philosophy and the Mechanical Arts* (London: Johnson J)
[2] Lewis G N 1926 *Nature* **118** 874
[3] Jönsson C 1961 *Z. Phys.* **161** 454
[4] Tonomura A, Endo J, Matsuda T, Kawasaki T and Ezawa H 1989 *Am. J. Phys.* **57** 117
[5] Barwick B, Gronniger G, Lu Y, Liou S Y and Batelaan H 2006 *J. Appl. Phys.* **100** 074322
[6] Frabboni S, Gazzai G C and Pozzi G 2007 *Am. J. Phys.* **75** 1053
[7] Frabboni S, Gazzai G C and Pozzi G 2008 *Appl. Phys. Lett.* **93** 073108
[8] Frabboni S, Gabrielli A, Gazzadi G C, Giorgi F, Matteucci G, Pozzi G, Cesari N S, Villa M and Zoccoli A 2012 *Ultramicroscopy* **116** 73
[9] Arndt M, Nairz O, Vos-Andreae J, Keller C, van der Zouw G and Zeilinger A 1999 *Nature* **401** 680
[10] Becker U 2011 *Nature* **474** 586
[11] Bach R, Pope D, Liou S and Batelaan H 2013 *New J. Phys.* **15** 033018
[12] Stolterfoht N *et al* 2001 *Phys. Rev. Lett.* **87** 023201
[13] Rolles D *et al* 2005 *Nature* **437** 711
[14] Drake G W F 2005 *Springer Handbook of Atomic, Molecular and Optical Physics* (Berlin: Springer)
[15] Cohen H D and Fano U 1966 *Phys. Rev.* **150** 30
[16] Ullrich J, Moshammer R, Dorn A, Dörner R, Schmidt L Ph H and Schmidt-Böcking H 2003 *Rep. Prog. Phys.* **66** 1463
[17] Schulz M and Madison D H 2006 *Int. J. Mod. Phys.* A **21** 3649
[18] Bransden B H and Joachain C J 1983 *Physics of Atoms and Molecules* (London: Longman Group)
[19] Fainstein P D, Ponce V H and Rivarola R D 1991 *J. Phys. B: At. Mol. Opt. Phys.* **24** 3091
[20] Stolterfoht N, DuBois R D and Rivarola R D 1997 *Electron Emission in Heavy Ion-Atom Collisions* (Berlin: Springer)
[21] Rivarola R D, Piacentini R D, Salin A and Belkić Dž 1980 *J. Phys. B: At. Mol. Phys.* **13** 2601
[22] Fainstein P D, Ponce V H and Rivarola R D 1988 *J. Phys. B: At. Mol. Opt. Phys.* **21** 287
[23] Corchs S E, Rivarola R D and McGuire J H 1993 *Phys. Rev.* A **47** 3937

[24] Galassi M E, Rivarola R D and Fainstein P D 2004 *Phys. Rev.* A **70** 032721

[25] Nascimento R F, Machado L E, Bielschowsky C E and Jalbert G 2008 *J. Phys. B: At. Mol. Opt. Phys.* **40** 225201

[26] Nascimento R F, Machado L E, Medina A, Bielschowsky C E and Jalbert G 2012 *Eur. Phys. J.* D **66** 225

[27] Járai-Szabó F, Nagy-Póra K and Nagy L 2009 *J. Phys. B: At. Mol. Opt. Phys.* **42** 245203

[28] Chowdhury U, Schulz M and Madison D H 2011 *Phys. Rev.* A **83** 032712

[29] Sisourat N, Caillat J, Dubois A and Fainstein P D 2007 *Phys. Rev.* A **76** 012718

[30] Sælen L, Birkeland T, Sisourat N, Dubois A and Hansen J P 2010 *Phys. Rev.* A **81** 022718

[31] Crothers D S F and McCann J F 1983 *J. Phys. B: At. Mol. Phys.* **16** 3229

[32] Gulyás L, Fainstein P D and Salin A 1995 *J. Phys. B: At. Mol. Opt. Phys.* **28** 245

[33] Dewangan D P and Eichler J 1986 *J. Phys. B: At. Mol. Phys.* **19** 2939

[34] Gayet R 1972 *J. Phys. B: At. Mol. Phys.* **8** 483

[35] Wang Y D, McGuire J H and Rivarola R D 1989 *Phys. Rev.* A **40** 3673

[36] Galassi M E, Rivarola R D, Fainstein P D and Stolterfoht N 2002 *Phys. Rev.* A **66** 052705

[37] Nagy L, Kocbach L, Póra K and Hansen J P 2002 *J. Phys. B: At. Mol. Opt. Phys.* **35** L453

[38] Walter M and Briggs J 1999 *J. Phys. B: At. Mol. Opt. Phys.* **32** 2487

[39] Fojón O A, Fernández J, Palacios A, Rivarola R D and Martín F 2004 *J. Phys. B: At. Mol. Opt. Phys.* **37** 3035

[40] Stolterfoht N *et al* 2003 *Phys. Rev.* A **67** 030702(R)

[41] Hossain S, Alnaser A S, Landers A L, Pole D J, Knutson H, Robison A, Stamper B, Stolterfoht N and Tanis J A 2003 *Nucl. Instr. Meth. Phys. Res.* B **205** 484

[42] Hossain S, Landers A L, Stolterfoht N and Tanis J A 2005 *Phys. Rev.* A **72** 010701(R)

[43] Hossain S 2003 private communication

[44] Stolterfoht N, Sulik B, Skogvall B, Chesnel J Y, Frémont F, Hennecart D, Cassimi A, Adoui L, Hissain S and Tanis J A 2004 *Phys. Rev.* A **69** 012701

[45] Misra D, Khadane U, Singh Y P, Tribedi L C, Fainstein P D and Richard P 2004 *Phys. Rev. Lett.* **92** 153201

[46] Misra D, Kelkar A, Kadhane U, Kumar A, Tribedi L C and Fainstein P D 2006 *Phys. Rev.* A **74** 060701(R)

[47] Laurent G, Fainstein P D, Galassi M E, Rivarola R D, Adoui L and Cassimi A 2002 *J. Phys. B: At. Mol. Opt. Phys.* **35** L495

[48] Stolterfoht N *et al* 1987 *Europhys. Lett.* **4** 899

[49] Misra D, Kelkar A, Kadhane U, Kumar A, Singh Y P and Tribedi L C 2007 *Phys. Rev.* A **75** 052712

[50] Ciappina M F and Rivarola R D 2008 *J. Phys. B: At. Mol. Opt. Phys.* **41** 015203

[51] Ciappina M F and Cravero W R 2006 *J. Phys. B: At. Mol. Opt. Phys.* **39** 2183

[52] Itatani J, Levesque J, Zeidler D, Niikura H, Pépin H, Kieffer J C, Corkum P B and Villeneuve D M 2004 *Nature* **432** 867

[53] Sakai H, Safvan C P, Larsen J J, Hilligsoe K M, Hald K and Stapelfeldt H 1999 *J. Chem. Phys.* **110** 10235

[54] Rosca-Pruna F and Vrakking M J J 2001 *Phys. Rev. Lett.* **87** 153902

[55] Dooley P W, Litvinyuk I V, Lee K F, Rayner D M, Spanner M, Villeneuve D M and Corkum P B 2003 *Phys. Rev.* A **68** 023406

[56] Larsen J J, Hald K, Bjerre N and Stapelfeldt H 2000 *Phys. Rev. Lett.* **85** 2470

[57] Sakai H, Minemoto S, Nanjo H, Tanji H and Suzuki T 2003 *Phys. Rev. Lett.* **90** 083001

[58] Alexander J S, Laforge A C, Hasan A, Machavariani Z S, Ciappina M F, Rivarola R D, Madison D H and Schulz M 2008 *Phys. Rev.* A **78** 060701

[59] Egodapitiya K N, Sharma S, Hasan A, Laforge A C, Madison D H, Moshammer R and Schulz M 2011 *Phys. Rev. Lett.* **106** 153202

[60] Dimopoulou C *et al* 2005 *J. Phys. B: At. Mol. Opt. Phys.* **38** 593

[61] Tachino C A, Galassi M E, Martín F and Rivarola R D 2009 *J. Phys. B: At. Mol. Opt. Phys.* **42** 075203

[62] Tachino C A, Galassi M E, Martín F and Rivarola R D 2010 *J. Phys. B: At. Mol. Opt. Phys.* **43** 135203

[63] Tachino C A, Galassi M E, Martín F and Rivarola R D 2011 *J. Phys.: Conf. Ser.* **288** 012026

[64] O-ohata K, Taketa H and Huzinaga S 1966 *J. Phys. Soc. Japan* **21** 2306

[65] Hehre W J, Stewart R F and Pople J A 1969 *J. Chem. Phys.* **51** 2657

[66] Frisch M J *et al* 1998 *Gaussian 98, revision A 11* (Pittsburgh, PA: Gaussian Inc.)

[67] Nagy-Póra K, Czipa L and Nagy L 2012 *Stud. UBB Phys.* **57** 49

[68] Tachino C A, Martín F and Rivarola R D 2012 *J. Phys. B: At. Mol. Opt. Phys.* **45** 025201

[69] Baran J L, Das S, Járai-Szábo F, Nagy L and Tanis J A 2007 *J. Phys.: Conf. Ser.* **58** 215

[70] Baran J L, Das S, Járai-Szábo F, Póra K, Nagy L and Tanis J A 2008 *Phys. Rev.* A **78** 012710

[71] Winkworth M, Fainstein P D, Galassi M E, Baran J, Dassanayake B S, Das S, Kayani A and Tanis J A 2009 *Nucl. Instr. Meth. Phys. Res.* B **267** 373

[72] Winkworth M, Fainstein P D, Galassi M E, Baran J, Das S, Kayani A, Dassanayake B S and Tanis J A 2009 *J. Phys.: Conf. Ser.* **163** 012044

[73] Nandi S, Agnihotri A N, Tachino C A, Rivarola R D, Martín F and Tribedi L 2012 *J. Phys. B: At. Mol. Opt. Phys.* **45** 215207

[74] Nandi S, Agnihotri A N, Kasthurirangan S, Kumar A, Tachino C A, Rivarola R D, Martín F and Tribedi L 2012 *Phys. Rev.* A **85** 062705

[75] Dey S, McCarthy I E, Teubner P J O and Weigold E 1975 *Phys. Rev. Lett.* **34** 782

[76] Zurales R W and Lucchese R R 1988 *Phys. Rev.* A **37** 1176

[77] Houamer S, Mansouri A, Cappello C D, Lahmam-Bennani A, Elazzouzi S, Moulay M and Charpentier I 2003 *J. Phys. B: At. Mol. Opt. Phys.* **36** 3009

[78] Wang S C 1928 *Phys. Rev.* **39** 579

[79] Weck P, Fojón O A, Hanssen J, Joulakian B and Rivarola R D 2001 *Phys. Rev.* A **63** 042709

[80] Stia C R, Fojón O A, Weck P, Hanssen J, Joulakian B and Rivarola R D 2002 *Phys. Rev.* A **66** 052709

[81] Brauner M, Briggs J S and Klar H 1989 *J. Phys. B: At. Mol. Opt. Phys.* **22** 2265

[82] Garibotti C R and Miraglia J E 1980 *Phys. Rev.* A **21** 572

[83] Stia C R, Fojón O A, Weck P, Hanssen J and Rivarola R D 2003 *J. Phys. B: At. Mol. Opt. Phys.* **36** L257

[84] Fojón O A, Stia C R and Rivarola R D 2011 *Phys. Rev.* A **84** 032715

[85] Senftleben A, Pflüger T, Ren X, Al-Hagan O, Najjari B, Madison D H, Dorn A and Ullrich J 2010 *J. Phys. B: At. Mol. Opt. Phys.* **43** 081002

[86] Kamalou O, Chesnel J-Y, Martina D, Frémont F, Hanssen J, Stia C R, Fojón O A and Rivarola R D 2005 *Phys. Rev.* A **71** 010702(R)

[87] Stolterfoht N 1971 *Z. Phys.* **248** 81
Stolterfoht N 1971 *Z. Phys.* **248** 92

[88] Murray A J 2005 *J. Phys. B: At. Mol. Opt. Phys.* **38** 1999

[89] Gao J F, Madison D H and Peacher J L 2005 *Phys. Rev.* A **72** 032721
[90] Fojón O A, Fernández J, Palacios A, Rivarola R D and Martín F 2004 *J. Phys. B: At. Mol. Opt. Phys.* **37** 3035
[91] Hargreaves L R, Colyer C, Stevenson M A, Lohmann B, Al-Hagan O, Madison D H and Ning C G 2009 *Phys. Rev.* A **80** 062704
[92] Prideaux A, Madison D H and Bartschat K 2005 *Phys. Rev.* A **72** 032702
[93] Gao J, Madison D H and Peacher J L 2005 *J. Chem. Phys.* **123** 204314
[94] Foster M, Madison D H, Peacher J L, Schulz M, Jones S, Fischer D, Moshammer R and Ullrich J 2004 *J. Phys. B: At. Mol. Opt. Phys.* **37** 1
[95] Milne-Brownlie D S, Foster M, Gao J, Lohmann B and Madison D H 2006 *Phys. Rev. Lett.* **96** 233201
[96] Casagrande E M S *et al* 2008 *J. Phys. B: At. Mol. Opt. Phys.* **41** 025204
[97] Chatterjee S, Misra D, Kelkar A H, Tribedi L, Stia C R, Fojón O A and Rivarola R D 2008 *Phys. Rev.* A **78** 052701
[98] Chatterjee S, Kasthurirangan S, Kelkar A H, Stia C R, Fojón O A, Rivarola R D and Tribedi L 2009 *J. Phys. B: At. Mol. Opt. Phys.* **42** 065201
[99] Misra D, Kelkar A, Kadhane U, Kumar A, Singh Y P, Tribedi L C and Fainstein P D 2007 *Phys. Rev.* A **75** 052712
[100] Fernández J, Fojón O A, Palacios A and Martín F 2007 *Phys. Rev. Lett.* **98** 043005
[101] Fojón O A, Stia C R and Rivarola R D 2012 *J. Phys.: Conf. Ser.* **388** 052035
[102] Baltenkov A S, Becker U, Manson S T and Msezane A Z 2012 *J. Phys. B: At. Mol. Opt. Phys.* **45** 035202
[103] Ozer Z N, Chaluvadi H, Ulu M, Dogan M, Aktas B and Madison D H 2013 *Phys. Rev.* A **87** 042704
[104] Misra D, Kelkar A, Kadhane U, Kumar A, Singh Y P, Tribedi L C and Fainstein P D 2007 *Phys. Rev.* A **75** 052712
[105] Misra D, Kelkar A, Kadhane U, Kumar A, Tribedi L C and Fainstein P D 2006 *Phys. Rev.* A **74** 060701(R)
[106] Fainstein P D, Gulyás L, Martín F and Salin A 1996 *Phys. Rev.* A **53** 3243
[107] Fojón O A, Stia C R and Rivarola R D 2006 *AIP Conf. Proc.* **811** 42
[108] Cherid M, Lahman-Bennani A, Zurales R W, Lucchese R R, Duguet A, Dal Cappello M C and Dal Cappello C 1989 *J. Phys. B: At. Mol. Opt. Phys.* **22** 3483
[109] Al-Hagan O, Kaiser C, Madison D H and Murray A J 2009 *Nature Phys.* **5** 59
[110] Dörner R, Mergel V, Jagutzki O, Spielberger L, Ullrich J, Moshammer R and Schmidt-Böcking H 2000 *Phys. Rep.* **330** 95
[111] Senftleben A, Al-Hagan O, Pflüger T, Ren X, Madison D H, Dorn A and Ullrich J 2010 *J. Chem. Phys.* **133** 044302
[112] Bellm S, Lower J, Weigold E and Mueller D W 2010 *Phys. Rev. Lett.* **104** 023202
[113] Chatterjee S, Agnihotri A N, Stia C R, Fojón O A, Rivarola R D and Tribedi L C 2010 *Phys. Rev.* A **82** 052709
[114] Fojón O A, Palacios A, Fernández J, Rivarola R D and Martín F 2006 *Phys. Lett.* A **350** 371
[115] Fernández J, Fojón O A and Martín F 2009 *Phys. Rev.* A **79** 043409
[116] Martín F 1999 *J. Phys. B: At. Mol. Opt. Phys.* **32** R197
[117] Bachau H, Cormier E, Decleva P, Hansen J E and Martín F 2001 *Rep. Prog. Phys.* **64** 1815
[118] Kolos W, Szalewicz K and Monkhorst H J 1986 *J. Chem. Phys.* **84** 3278
[119] Chung Y M, Lee E M, Masuoka T and Samson J A R 1993 *J. Chem. Phys.* **99** 885
[120] Dill D 1976 *J. Chem. Phys.* **65** 1130
[121] Samson J A R and Cairns R B 1965 *J. Opt. Soc. Am.* **55** 1035
[122] Kaplan I G and Markin A P 1969 *Sov. Phys. Dokl.* **14** 36
[123] Picca R D, Fainstein P D, Martiarena M L and Dubois A 2008 *Phys. Rev.* A **77** 022702
[124] Picca R D, Fainstein P D, Martiarena M L, Sisourat N and Dubois A 2009 *Phys. Rev.* A **79** 032702
[125] Semenov S K and Cherepkov N A 2003 *J. Phys. B: At. Mol. Opt. Phys.* **36** 1409
[126] Wallace S and Dill D 1978 *Phys. Rev.* B **17** 1692
[127] Akoury D *et al* 2007 *Science* **318** 949
[128] Canton S E, Plésiat E, Bozek J D, Rude B S, Decleva P and Martín F 2011 *Proc. Natl Acad. Sc. USA* **108** 7302